Ancient TL

A periodical devoted to Luminescence and ESR dating

Volume 31 No.1   June 2013

Ancient TL

Started by the late David Zimmerman in 1977

Ancient TL

A periodical devoted to Luminescence and ESR dating

Web site: http://www.aber.ac.uk/ancient-tl

Quantification of cross-bleaching during infrared (IR) light stimulation

Sebastian Kreutzer [1,2,*], Daniela Hülle [3], Kristina Jørkov Thomsen [4], Alexandra Hilgers [3], Annette Kadereit [5], Markus Fuchs[1]

[1]Department of Geography, Justus-Liebig-University Giessen, 35390 Giessen, Germany
[2]Geographical Institute, Geomorphology, University of Bayreuth, 95440 Bayreuth, Germany
[3]Institute of Geography, University of Cologne, 50923 Cologne, Germany
[4]Center for Nuclear Technologies, Technical University of Denmark, Risø Campus, DK-4000 Roskilde, Denmark
[5]Heidelberger Lumineszenzlabor, Geographisches Institut der Universität Heidelberg, Im Neuenheimer Feld 348, 69120 Heidelberg, Germany

[*]corresponding author: sebastian.kreutzer@geogr.uni-giessen.de

_____

Abstract

The cross-bleaching behaviour of automated Risø TL/OSL (DA-12, DA-15, DA-20) luminescence readers is investigated. By design, up to 24 or 48 aliquots can be stored on a carousel in a single measurement chamber. Due to this construction, irradiation or illumination on one sample may affect the adjacent position resulting in systematic errors.

Previously reported for blue LEDs, such cross-talk (cross-bleaching/illumination) has never been quantified explicitly for the infrared (IR) LEDs, although they are intensively used in IRSL measurements of e.g. feldspar and polymineral samples. In IRSL measurements of feldspar or polymineral samples it is important to keep the time constant between the (midpoint of the) irradiation and the subsequent read out to avoid the malign effects of anomalous fading in laboratory constructed dose response curves. This may be achieved by running all measurements for equivalent dose estimation on a single sample before moving to a subsequent sample (e.g. by using the "run 1 at a time" option in the Risø sequence editor). However, if the measurement sequence is not designed carefully, then using this option may result in a significant depletion of the natural signal on subsequent samples. Here we investigate the size of this reduction due to cross-bleaching from the IR diodes and quantify the cross-bleaching for 10 different Risø TL/OSL readers produced between 1994 and 2011. We find that cross-bleaching from the IR diodes is worse than from the blue diodes. Using the "run 1 at the time" option can result in significant dose underestimation (1) if the sequence is not split into different sets, or (2) if samples are not placed on every 2nd position. In addition, a newly designed flange for the optical unit of the TL/OSL reader is presented which appears to reduce cross-bleaching significantly.

Keywords: Cross-bleaching, IRSL, polymineral, feldspar, instrumentation, improved luminescence-reader design

Introduction

Dating of sediments using optically stimulated luminescence (OSL) was introduced in 1985 by Huntley et al. (1985) for quartz and using infrared stimulated luminescence (IRSL) for K-feldspar by Hütt et al. (1988). The introduction of the single-aliquot regenerative-dose (SAR) protocol (Murray and Wintle, 2000) enabled a wide range of dating applications in a short time span. Due to the development of automated luminescence dating systems (e.g. Bøtter-Jensen, et al. 2003, Bøtter-Jensen 1997) OSL and IRSL dating results have been produced more and more rapidly.

The commonly used Risø TL/OSL readers accommodate up to 48 individual samples, which are located in the measurement chamber on a sample carousel (Fig. 1). The distance between the centres of neighbouring (adjacent) samples is 17 mm. For older readers with only 24 sample positions this distance is 32 mm. In the standard Risø TL/OSL reader, illumination is achieved using seven clusters of LEDs mounted concentrically in a ring-shaped holder (stimulation head). Each cluster contains seven LEDs and each individual diode is focused at the sample.
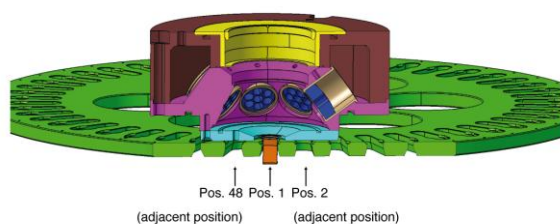
Figure 1: *Technical drawing of the stimulation head and the sample carousel of a Risø TL/OSL reader (DA-15, DA-20).*

The stimulation head normally contains three IR (870 Δ 40 nm) and four blue (470 Δ 30 nm) LED clusters. For illumination the sample is lifted up from the sample carousel into the stimulation head through a circular opening (ø 15.5 mm) in the bottom flange of the stimulation head (see Fig. 1 and Fig. 5). A consequence of the close proximity of the adjacent sample positions and the illumination geometry is that adjacent samples are also optically stimulated during illumination. This is known as cross-bleaching (cross-illumination, optical cross-talk) and has previously been determined to be 0.006% (Bøtter-Jensen et al. 2000) or 0.014% (Bray et al. 2002) for the blue LEDs. Although these cross-bleaching values appear small they may significantly reduce the luminescence signal of samples on adjacent (i.e. subsequent) positions if long illumination times are employed or if all illuminations in the measurement sequence are carried out on a single position before measurements of the adjacent sample (a long total/cumulative stimulation time). Bray et al. (2002) showed that if a sample is illuminated for a total of 1400 s by blue LEDs then the first signal measured from the adjacent sample position may be reduced by ~18% in a standard SAR run. In OSL dating procedures the first signal read out in a SAR sequence is the natural signal of a sample, and hence cross-bleaching will lead to age-underestimation. However, this is generally not an issue for quartz measurements because there is no demand that the time between irradiation and readout is kept constant, and so the illumination time of any one sample is typically ~40 s before the adjacent sample is measured and thus the effect of cross-bleaching is assumed to be negligible.

In contrast, the stimulation time on one position for feldspar measurements is markedly longer (e.g. up to 240 s Kadereit et al., 2010) and many feldspars have been shown to suffer from anomalous fading (e.g. Wintle, 1973; Spooner, 1994). Thus it is important to keep the time elapsed between irradiation and readout fixed. This is easily accomplished using the "run 1 at

a time" option[1] in the Risø sequence editor but if care is not taken in the design of the measurement sequence cross-bleaching may be a significant problem.

In this work, we report cross-bleaching values measured for the IR LEDs on 10 different Risø TL/OSL readers produced between 1994 and 2011. The cross-bleaching values obtained for the IR LEDs are compared with values for blue LEDs from the literature and with values determined by our own measurements. We further investigate the effect which cross-bleaching may have on equivalent dose determination if this issue is not kept in mind when designing the measurement sequence. Finally, we show that the new stimulation head flange, developed by Risø, reduces the cross-bleaching significantly.

Experimental design
Instrumentation

Cross-bleaching was investigated for Risø TL/OSL (DA-12, DA-15, DA-20) readers. All readers are equipped with bialkali photomultiplier tubes (EMI 9235Q) and ^{90}Sr/^{90}Y β-sources. The luminescence in the UV/blue band (polymineral and potassium rich feldspar, infrared stimulation) was measured with a 3 mm Chroma D410/30x interference filter (410 Δ 30 nm) or a blue filter pack (390 Δ 60 nm, 4 mm Corning 7–59 in combination with 2 mm Schott BG 39). For the UV band (quartz, blue stimulation) a 7.5 mm Hoya U340 glass filter (290–370 nm) was used.

IRSL measurements were done at 50°C for 100s after a preheat of 250°C for 60 s. In between the various SAR cycles (L_x and T_x) a hotbleach at 280°C for 100 s was used. Measurements of the quartz OSL signal using blue stimulation were carried out at 125°C for 100 s after a preheat of 260°C for 10 s. Both IR and blue stimulated signals reported here have been summed using the initial 0.5 s of the decay curves after subtraction of the last 10 s of the shine-down curve. For the signal curves (direct stimulation, Fig. 2b) only the first 20 s are recorded. Table 2 shows relevant data for the various readers investigated in this work.

Samples

All measurements were carried out on sedimentary samples. To avoid a dependency of the results on a single sample, different natural coarse grain (potassium feldspar, quartz) and fine grain (polymineral, quartz) samples were used. However, the cross-bleaching results seem not to be markedly affected by the chosen samples. A list of all investigated samples with their references is given in the supplementary information (Table S1).

---

[1] All operations in a given set are carried out on a single sample before any operation is carried out on the next sample.

Table 1: *Cross-bleaching protocol.*

Cross-bleaching protocol

To estimate the cross-bleaching value on an adjacent sample position a blank sample holder was placed on position 1 (measurement position) and a sample on position 2 (adjacent position). Sample holders were either cups or discs (ø 9.7 mm; stainless steel or aluminium). Initially the sample was repeatedly dosed, preheated and read out to stabilize the aliquot in terms of sensitivity change. The full sequence used to estimate the cross-bleaching is given in Table 1. The basic structure of the sequence is that the sample is dosed and preheated but before read out, the blank sample holder (measurement position) is illuminated for a time t_x varying between 0 and t_{max} (for most estimates t_{max} is 4,800 s but in some cases it was increased to 15,000 s). Subsequent to each illumination the sample on the adjacent position is read out (L_x) followed by a test dose (T_x) measurement. In between the various SAR cycles (L_x/T_x) the sample was bleached at 280°C for 100 s. Three recycling points were inserted to ensure that any sensitivity change was corrected adequately. To eliminate the effects of anomalous fading the time elapsed between irradiation and read out (L_x) was kept constant by inserting a pause of duration x = t_{max} – t_x. In practice this pause was split in two parts of equal duration, one inserted before and one after the illumination of the empty measurement position. The sequences were run using the "run 1 at a time" option.

In order to derive a value for cross-bleaching, the observed reduction of the luminescence signal of the sample on the adjacent position is compared to that measured by direct stimulation of the same sample (Table 1 part B, Fig. 2b).
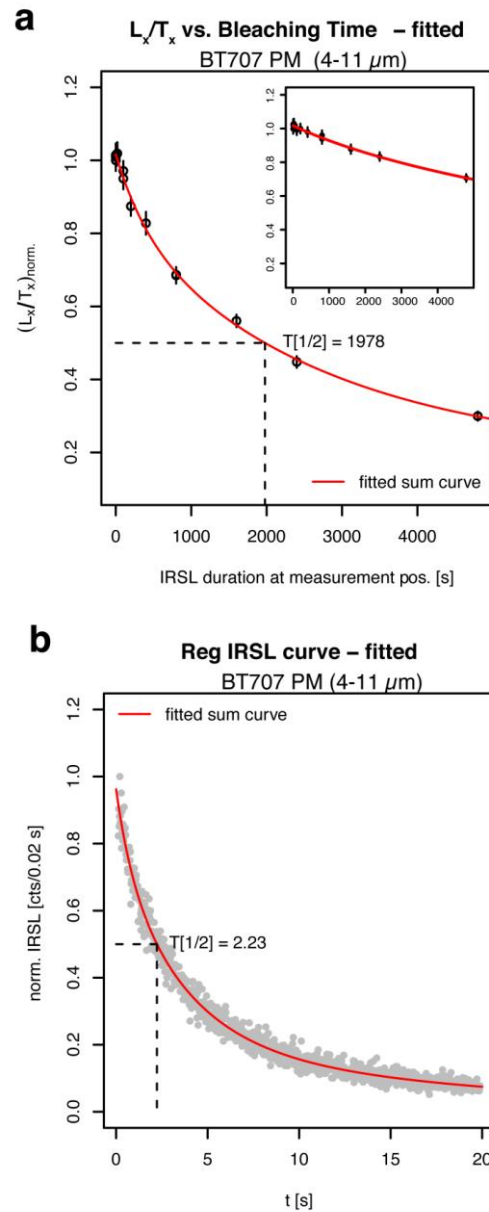
Figure 2: *Normalized L_x/T_x values shown as a function of IR illumination time for the reader with the highest relative cross-bleaching value. (a) Fitted L_x/T_x on the adjacent position (y-axis), each gained with the cross-bleaching protocol (Part B, protocol Table 1) after a respective illumination time on the measurement position (x-axis). L_x/T_x values normalized to the first value and then fitted with a multi-exponential function (n_{max} = 3). The halftime (T[1/2]) is derived iteratively. The obtained halftime from (a) is then compared with the halftime from (b) which is signal curve fitted to the IRSL decay curve data of the sample illuminated for 20 s (part B protocol, Table 1). The inset shows the fitted L_x/T_x values obtained for a reader with lower cross-bleaching behaviour.*

All L_x/T_x ratios were plotted as a function of illumination time and fitted (1) using either a multi-exponential function, where the number of components varied between 1 and 3 (reader ID 45 to ID 262) or (2) using an inverse power law function (reader ID 326). In the first approach the halftime of the fitted curve of the L_x/T_x ratios is compared to the halftime determined from the decay curve observed from direct stimulation (signal curve). In the second approach, the parameters in the inverse power law function fitted to the decay curve from direct stimulation are used to determine the equivalent loss resulting from cross-bleaching. In practice, these two approaches do not result in significantly different cross-bleaching values. Nevertheless, it should be noted that using a multi-exponential function for fitting is not related to any physical model. Details on the quantification procedures are given in the supplementary information (Section 1 supplement).

Measuring the effect of cross-bleaching on dose estimation

Cross-bleaching values are primarily a technical characteristic of a reader. They do not give any information on the degree of the depletion of a luminescence signal or on the corresponding reduction of the equivalent dose (D_e) of a dating sample. In the literature (Bray et al. 2002) it has already been demonstrated that cross-bleaching from the blue LEDs can reduce the estimated equivalent dose significantly if the entire dose-estimation sequence is carried out on a single aliquot before the next aliquot is measured. Here, we report the results from a similar experiment using the IR LEDs.

Two feldspar samples (US-C, KG-1) were heated to 500°C for two hours to completely eliminate the IRSL signal before giving to five portions of each sample gamma (^{60}Co) doses of 4.45 Gy, 8.9 Gy, 13.35 Gy, 26.7 Gy and 40.5 Gy, respectively.

12 aliquots of each gamma-dosed portion were subsequently measured using a routine SAR IRSL protocol with six regeneration doses and IR stimulation at 50°C for 300 s. The sequence was written in a single set in the Risø sequence editor and the "run 1 at a time" option was chosen. This means that the first aliquot was stimulated for a total of 4,200 s (14 × 300 s), before the natural signal of the subsequent aliquot was read out. For each portion irradiated with a given gamma-dose, aliquots were placed at positions 1–4, 10–13 and 20–23. Thus, there are three measurement positions (1, 10, 20) for which optical cross-bleaching is assumed to be insignificant, and nine measurement positions for which cross-bleaching is likely to affect the dose estimate. Sample US-C was measured on a single reader (ID 262, gamma-dose portions as stated above) to investigate a potential dose-dependency,

whereas sample KG-1 was measured on three different readers (ID 262, 133 and 45) to investigate the variability of cross-bleaching characteristics between individual readers.

Results
Cross-bleaching values

In Fig. 2a the IRSL L_x/T_x measurements are shown as a function of the illumination time for reader ID 189. For this particular reader, 4,800 s of illumination results in a depletion of the signal of the adjacent aliquot of ~70%. For the second nearest position an illumination of 4,800 s results in signal depletion of ~5%. Both data sets have been fitted using a linear combination of exponentially decaying functions. In Fig. 2b a decay curve obtained under direct stimulation is shown. In summary, for this particular reader, cross-bleaching values of 0.128 ± 0.017% (n=4) and 0.003% (n=1) were derived for the nearest (adjacent) and second nearest (adjacent of the adjacent) position, respectively. These cross-bleaching values are significantly higher than what has been reported for the blue LEDs in the literature before and what has been observed for the other readers investigated in this study. The inset shows the fitted L_x/T_x-values obtained for a reader with lower cross-bleaching behaviour (ID 150). All derived cross-bleaching values are summarized in Table 2. Errors of the cross-bleaching values were only given, if at least two repetitive measurements were carried out (see Table 2). Error bars show the standard deviation.

Our experiments show that the cross-bleaching value for the IR LEDs on the adjacent position range from <0.0001% (ID 60) to 0.1279 ± 0.0167% (ID 189). In comparison, the cross-bleaching values derived for the blue LEDs range from 0.0019% (ID 150) to 0.0176% (ID 189). Thus, in all cases the cross-bleaching resulting from the IR LEDs is approximately one order of magnitude larger than that from the blue LEDs (Table 2, Fig. 3).

The lowest cross-bleaching values were observed for the oldest readers (ID 45 and ID 60), which both accommodate sample carousels with only 24 sample positions (as opposed to 48 for all readers produced after 1996). For these sample carousels, the distance between the centres of adjacent sample positions are 32 mm (compared to 17 mm on a carousel accommodating up to 48 samples

The derived cross-bleaching values for a given type of stimulation source (IR- or blue LEDs) vary markedly also between readers and they even scatter for a single sample on the same reader (e.g. ~13% difference between repetitive determinations of the IR cross-bleaching value for reader ID 189, Fig. S1). We further observed a dependency of the IR cross-bleaching values on the chosen signal integral

Risø ID	Year	Type	Head	Sample Carousel	Blue Power [mW cm^{-2}]	IR Power [mW cm^{-2}]	Sample Carrier	Sample Code	Stimulation	Cross-Bleaching			
										Nearest [%]	Nearest Error [%]	2nd Nearest [%]	2nd Nearest Error [%]
45	1994	DA-12	std	24			steel discs	ME S2	IR	0.0065	NA	NV	NV
60	1996	DA-12	SG	24	53	140	steel discs	ME S2	IR	<0.0001	NA	NV	NV
98	2000	DA-15	SG	48	89	147	steel discs	ME S2	IR	0.0167	NA	NV	NV
133	2002	DA-15	SG	48		140	steel discs	ME S2	IR	0.0138	NA	NV	NV
150	2003	DA-15	std	48	40	120	Al discs	BT707, BT711	IR	0.0239	0.0042	NV	NV
							Al discs	BT620	Blue	0.0019	NA	<0.0001	NA
189	2005	DA-15	std	48	36	123	Al discs	BT707	IR	0.1279	0.0167	0.003	NA
							Al discs	BT714, BT620	Blue	0.0176	0.0003	NA	NA
240	2008	DA-20	std	48	45	131	Al discs	HDS-493m, HBII	IR	0.0387	NA	NV	NV
245	2008	DA-20	std	48	47	137	Al discs	HDS-499m, HBII	IR	0.0398	NA	NV	NV
							Al cups	BolivienQ 1409 LM1	Blue	0.0028	0.0004	NV	NV
262	2008	DA-20	std	48	80	128	steel discs	ME S2	IR	0.0296	0.0071	NV	NV
326	2011	DA-20	std	48	78	157	steel discs	914807	Blue	0.0020	NA	0.00016	NA
							steel cups	970425	IR	0.0160	NA	0.0004	NA

Notes

Year - production year. Some of the readers have been upgraded since production.

Stimulation head – 'std' is the standard stimulation head, 'SG' is a special stimulation head used on readers with a single grain attachment

Sample carousel - the number of available sample positions

Stimulation - stimulation light source (blue and IR). The IR stimulations were detected in the blue range, whereas the blue stimulated signals were detected in the UV range

NA - Not Available (not calculated in cases were the measurement was repeated only once)

NV - No Value (not measured)

Table 2: *Reader characteristics and cross-bleaching results.*
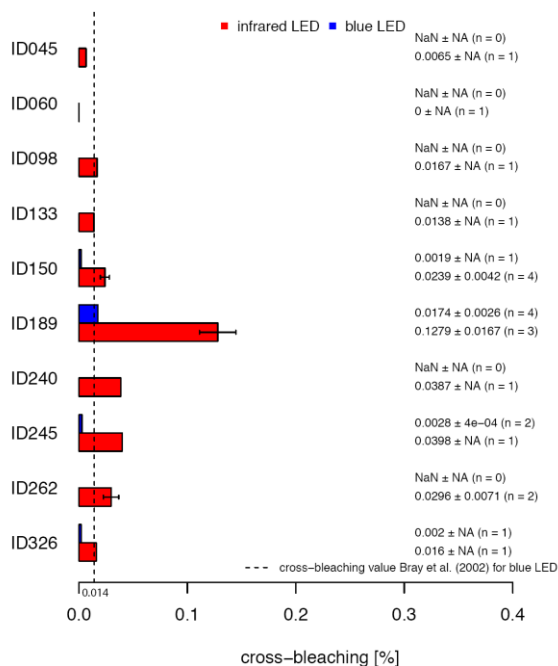
Figure 3: *Cross-bleaching on the adjacent position for IR- and blue LEDs of the investigated readers. If only one measurement was carried out, no error is given. The dashed line denotes the cross-bleaching value for blue LEDs (0.014%) published by Bray et al. (2002).*

Figure 4: *Measured dose plotted as a function of given dose. All results derived by using the 'run 1 at a time' option for the measurement positions 1–4, 10–13 and 20–23 on reader ID 262 (model DA-20). The aliquots on the positions 1, 10 and 20, which are not affected by cross-bleaching, are displayed as black circles; all other aliquots (influenced by cross-bleaching) are given as grey rectangles and triangles. Also shown is the 1:1 line (black) and the ± 10% lines (dotted lines).*

(Fig. S2) which decrease with longer signal integrals. However, for all experiments the chosen signal integral was kept constant (see Sec. 2.3).

Except for a single outlier (ID 189) the DA-15 readers (produced between 1997 and 2005) yield mean optical cross-talk values for the blue LEDs of 0.017 ± 0.003% (n=3) which is similar within errors to the cross-bleaching value of 0.014% reported by Bray et al. (2002) for the blue LEDs. The highest cross-bleaching values for the IR LEDs were measured for the newest DA-20 series (produced since 2006) with a mean value of 0.028 ± 0.002% (n=3) for discs. Thus, it would appear that the cross-talk of the IR LEDs have increased by a factor of two. In Table 2 the power density at the sample position at 100% LED power is given for each reader and it is apparent that there is no correlation between the power of the IR LEDs and the measured relative optical cross-talk. This observation seems to be confirmed by an additional experiment on reader ID 189 using a polymineral fine grain sample (BT714). For this sample, no correlation was found between IR stimulation power densities of 31 mW cm^{-2} (25% LED power) and 62 mW cm^{-2} (50% LED power), respectively, and the observed cross-bleaching values (data not shown). No dependency of the IR cross-

bleaching intensity on the type of stimulation units (i.e. standard or single-grain) was observed.

Effect of cross-bleaching on dose estimation

Figure 4 shows that the measured equivalent doses for sample US-C measured on reader ID 262 reproduce the given dose within ± 10% for the three aliquots on the positions 1, 10 and 20. The tendency of D_e underestimation for the larger doses may be interpreted in terms of fading as the time span between irradiation and measurement was a couple of weeks. In contrast, the measured D_e values of all nine aliquots without an empty position to the left are systematically lower than the given dose. The relative underestimation of ~36 ± 3.2% is not dependent on the given dose. The reason for this is that the stimulation time, and thus the time when cross-bleaching occurs, is constant. Furthermore, it can be deduced that cross-irradiation does not appear to be significant. If it was, we would expect to observe dose-dependent differences.

Although, these effects have not been explicitly investigated in this study, in addition two samples of cross-irradiation measurements using a quartz sample on reader ID 240 are provided in the supplementary information (Figs. S4 and S5). For this reader, the cross-irradiation was found to be ~0.01% on the adjacent position and ~0.001% on the 2nd adjacent position.

Stimulation	Mineral	Sample Carrier	Flange	t_{max} [s]	Nearest [%]	2nd nearest [%]
Blue	Q	steel disc	std	15000	0.00200	0.00016
Blue	Q	steel cups	std	15000	0.00100	0.00003
Blue	Q	steel cups	new	15000	0.00005	
Blue	KF	steel cups	new	10000	0.00010	
IR	KF	steel cups	std	4800	0.01600	0.00040
IR	KF	steel cups	new	10000	0.00100	
IR	KF	steel disc	new	10000	0.00300	

Table 3: *Cross-bleaching results on reader ID 326 using the standard and the new bottom flange.*

However, it should be noted that this value is dependent on the built in irradiation source and therefore may vary from reader to reader (compare e.g. Thomsen et al., 2006; Bray et al., 2003; Bøtter-Jensen et al., 2000; Markey et al. 1997).

The second sample, KG-E, was measured on three different readers (ID 262, 133 and 45). For reader ID 262 a D_e underestimation of $37 \pm 3.3\%$ supports the reduction determined for sample US-C above. From the typical decay curves of both samples, it can be deduced that this reduction is equivalent to the depletion caused by ~1.7 s of direct stimulation. Dividing these 1.7 s by the total illumination time (4,200 s) of a complete SAR-protocol, the IR cross-bleaching value is estimated to be ~ 0.04%.

For reader ID 133 the underestimation of 11–18% corresponds to ~0.58 s of direct stimulation giving an estimated cross-bleaching value of ~ 0.014%.

Thus the obtained cross-bleaching values for reader ID 262 and ID 133 are of a similar order of magnitude as the values obtained by the measurements described above.

For reader ID 45 cross-bleaching causes a D_e underestimation of 9–15% giving an estimated cross-bleaching value of 0.011%.[2] A smaller cross-bleaching value was expected for this reader as it has a 24 position sample carousel, i.e. adjacent sample positions are further apart.

Our measurements indicate that sequences should not be written in a single set (writing measurements steps within one single row in Sequence Editor), if the "run 1 at a time option" is chosen or long illumination times on a measurement position are applied. They also show that cross-bleaching may vary significantly from reader to reader.

Instrument modification to reduce cross-bleaching

To reduce the effect of cross-bleaching a new flange has been designed by Risø which instead of a circular opening has an opening shaped as the lift

itself (see Fig. 5). A series of experiments were undertaken using reader ID 326 (produced in 2011) to assess the cross-bleaching using this new flange. The results are presented in Table 3 and can be summarised as follows: (1) It appears that by using stainless steel cups instead of stainless steel discs the cross-bleaching value is reduced by a factor of ~ 2.5. (2) The cross-bleaching value for the second nearest position is ~4% of the value from the adjacent (nearest) position. (3) These measurements confirm the previous observation that the cross-bleaching resulting from the IR LEDs is an order of magnitude larger than that from the blue LEDs. Finally, the results indicate that the new flange reduces cross-bleaching by a factor of ~20 to a value of 0.001% for the IR LEDs. The corresponding value for the blue LEDs is 0.00005%. The new flange is now the standard flange for all readers produced from the middle of 2012.

Discussions

Our results show that cross-bleaching varies significantly between the investigated readers. The differences are only partly correlated with the type series. For the DA-12 series, for which the distance between the centres of adjacent samples is 32 mm on the carousels with 24 positions one would a priori expect cross-bleaching to be negligible. This was only confirmed for one reader (ID 60). For the second investigated DA-12 reader (ID 45), however, we measured an optical cross-talk of 0.0065% indicating that cross-bleaching can be relevant also for the readers of the DA-12 series. This agrees with Bøtter-Jensen et al. (2000) who report on an improved lift mechanism for the at that time newly introduced DA-15 series, which reduced cross-bleaching as compared to the older DA-12 readers. Therefore, an old lift mechanism (differences in the uplift height) may be responsible for the observed cross-bleaching value of reader ID 45 that was not confirmed for reader ID 60. This reader, however, has been subjected to technical modifications (e.g. single grain attachment) over the years. The potential for anomalous fading (e.g. Wintle 1979; Visocekas

---

[2]Note that this value might not be comparable to the value derived by the cross-bleaching protocol in Table 1 because the stimulation unit was modified after the measurements described here.
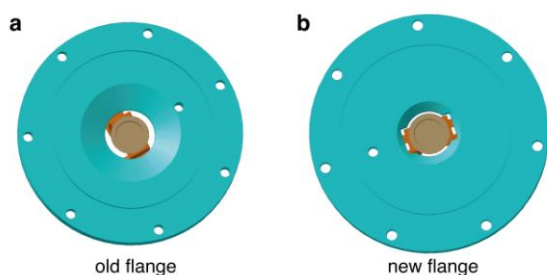
Figure 5: *Old (a) and new (b) bottom flange of the Risø reader. The opening has been minimized to reduce optical cross-talk.*

1985) to cause any signal loss was minimised by the sequence design and should therefore not be responsible for the signal loss observed on the DA-12 reader (ID 45).

Furthermore, it should be noted that our results for these readers are based on single measurements (one per reader). Due to technical modifications on reader ID 45 after the experiment the measurement could not be repeated.

For the DA-15 and DA-20 readers (excluding reader ID 189) we obtained a mean IR cross-bleaching value of 0.026% with a standard deviation of 0.011% consistently in the same order of magnitude as all investigated readers except for reader ID 189. Our findings indicate that the obtained IR cross-bleaching value of 0.1279 ± 0.0167% for this particular reader is not normally expected. As described in the introduction (see Fig. 1) the sample is lifted into the stimulation head through a circular opening in the bottom flange of the stimulation head. The differences are likely to arise from differences in how high the sample is lifted into the stimulation head, from the distance of the sample carousel with respect to the lid and/or from the thickness of the bottom flange. However, the actual reason for the observed behaviour remains unknown so far.

Surprisingly, the cross-bleaching value also varied for an identical sample on one reader and to a greater extent between assumed similar readers for one sample. Using an identical sample on one reader the measurement conditions were kept constant. Therefore it is likely that the differences result from the method applied for the calculation of the cross-bleaching value. The halftime of the obtained L_x/T_x-values on the adjacent position is compared with the halftime of a directly measured decay curve. Both halftimes are mathematically derived from previously fitted functions. Therefore, any (stochastic) variation in the fitted curve shapes yield different halftimes and cross-bleaching values.

Furthermore, our results show that the optical cross-talk for the IR LEDs is significantly higher than

that for the blue LEDs. The reasons for this observation could not be further investigated in this study and may reflect differences in the stimulation geometry and/or the optical characteristics of the LEDs.

Of more practical relevance might be the implications of the deduced, somehow artificial, and apparently highly reader-specific, cross-bleaching values. Our results suggest (e.g. Table 2) that the optical cross-talk of the IR LEDs on the Risø TL/OSL readers can be significant in routine dating applications, if care is not taken when designing the measurement sequences. In this respect, the most important question is: How much (cumulative/total) stimulation time on the measurement position is acceptable for a given threshold value of signal reduction on the adjacent position? To account for this question two normalized typical natural decay curves (BT711, fine grain, polymineral and quartz) measured at 90% LED power (IR and blue LED) were plotted against the cumulative stimulation time on the measurement position for given cross-bleaching values of 0.02% (IR LED) and 0.002% (blue LED). The results are shown in Fig. S3. Based on a fitted inverse power law (IR LED, polymineral sample, Fig. S3a) and a single exponential function (blue LED, quartz, Fig. S3b) the cumulative stimulation time on the measurement position for a given value of signal reduction on the adjacent position (1%, 10%, 25%, 50%) were calculated. For the fitting the first five seconds of the decay curve of the polymineral sample and the first two seconds of that of the quartz sample were used respectively. For example: For a signal reduction of 25% of the polymineral sample on the adjacent position, ~5168 s of IR stimulation (90% LED power) on the measurement position are needed (polymineral, Fig. S3a). Our considerations allow a calculation of all possible combinations of cumulative stimulations times on the measurement position and cross-bleaching values for a presumed threshold value of the signal reduction (isoline).

Figure 6 shows the 1% to 5% signal reduction isolines of a typical polymineral (IR stimulation, Fig. 6a) and quartz (blue stimulation, Fig. 6b) fine grain sample (BT711) for a realistic range of cross-bleaching values. Considering the overall precision of the cross-bleaching measurements the allowed value of stimulation time on the measurement position for a given value of signal reduction can be read off with sufficient accuracy from the figure. Thus, an assumed cross-bleaching value for the IR LEDs of 0.03% allows a stimulation time of ~100 s on the measurement position if a signal reduction of 1% on the adjacent position is accepted. Using the newly designed bottom flange, or every 2nd position on the sample carousel, in case the new flange has not yet
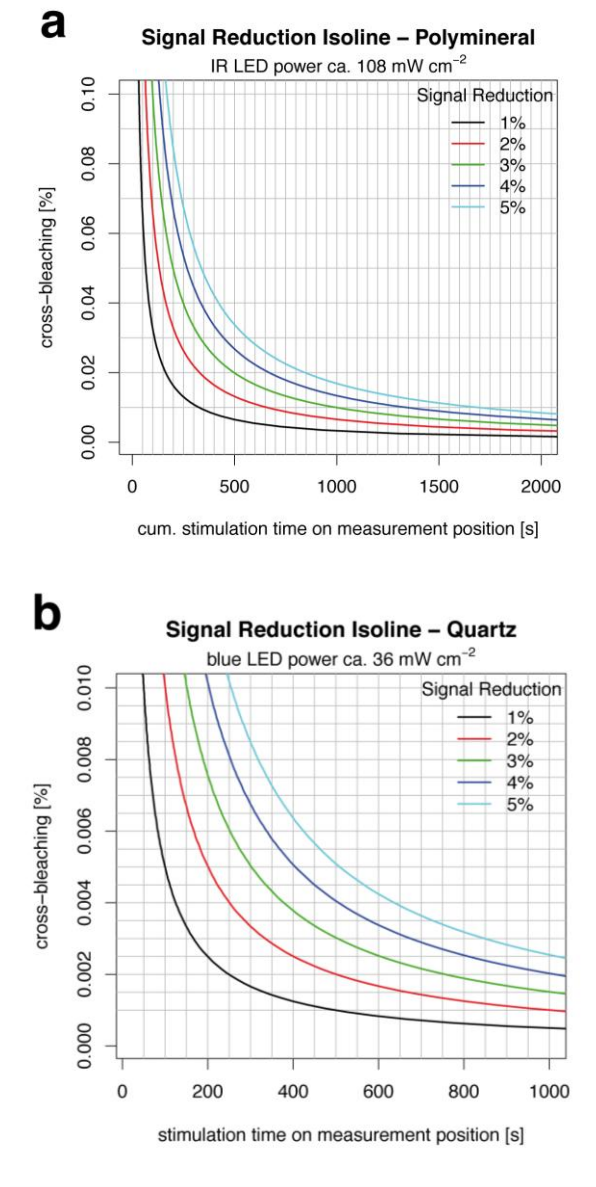
Figure 6: *Signal reduction on adjacent position vs. cross-bleaching values. Corresponding isolines for five hypothetically tolerated thresholds (1% to 5%) by cross-bleaching on the adjacent position. The lines represent all possible combinations of cumulative stimulation times (up to 2000s for IR stimulation) on the measurement position (x-axis) and cross-bleaching values of a reader (y-axis) for constant value of signal reduction. The signal-reduction isolines for a typical polymineral (a) and quartz (b) fine grain sample are shown using IR stimulation and blue stimulation respectively. Note that the shapes of the isolines depend slightly on the absolute power density of the stimulation LEDs. For further details see main text.*

been installed, a cross-bleaching value of <0.003% for the IR LEDs can be assumed. For the same amount of tolerated signal reduction, this allows stimulation times at least larger by a factor of ten. Thus cross-bleaching will become negligible for ordinary SAR-measurements.

In summary, for routine dating applications an appropriate measurement sequence design or the use of every 2nd position is considered as adequate to reduce any unwanted malign effect of cross-bleaching below the detection threshold.

Nevertheless, it is worth mentioning that the cross-bleaching values were measured using a blank sample carrier on the measurement position. Any sediment on the sample carriers may cause different (material dependent) scattering effects. Such effects have not been investigated in the presented study.

Conclusions

In this study the cross-bleaching (optical cross-talk) of the IR LEDs for the adjacent position has been investigated on various types of Risø TL/OSL readers. For the quantification three different methods were applied. The results were compared with findings from the literature and our own measurements of the cross-talk of the blue LEDs on the same reader. In addition, a newly designed flange to reduce the cross-bleaching was tested and the results were compared with the measurements run carried out using the standard flange. In summary:

1. We confirm that cross-bleaching exists for the IR LEDs on almost all investigated readers (~0.026% for DA-15 and DA-20 readers).
2. Our findings indicate that the cross-bleaching is significantly higher (ca. one order of magnitude) for the IR than for the blue LEDs.
3. The relative cross-bleaching seems to be independent of the stimulation power.
4. The cross-bleaching value varies with the used sample carrier and is observed to be higher for steel discs than for steel cups.
5. The newly designed bottom flange reduces the cross-bleaching by a factor of ~20 resulting in negligible signal reduction by cross-bleaching on the adjacent position.
6. The cross-bleaching effect can lead to significant age underestimations if care is not taken in the measurement-sequence design. It is therefore highly recommended to split the sequence in different sets when using the "run 1 at a time" option or to use only every 2nd measurement position on the sample carousel (for an assumed cross-bleaching value <0.0001% on the 2nd nearest position). A sequence template splitting up the steps in different sets is provided as supplementary data on the *Ancient TL* website.

Supplementary Information for this article is available at www.aber.ac.uk/ancient-tl

References

Bray, H.E., Bailey, R.M., Stokes, S. (2002). Quantification of cross-irradiation and cross-illumination using a Risø TL/OSL DA-15 reader. Radiation Measurements 35: 275–280.

Bøtter-Jensen, L. (1997). Luminescence techniques: Instrumentation and methods. Radiation Measurements 27: 749–768.

Bøtter-Jensen, L., Andersen, C.E., Duller, G.A.T., Murray, A.S. (2003). Developments in radiation, stimulation and observation facilities in luminescence measurements. Radiation Measurements 37: 535–541.

Bøtter-Jensen, L., Bulur, E., Duller, G.A.T., Murray, A.S. (2000). Advances in luminescence instrument systems. Radiation Measurements 32: 523–528.

Huntley, D.J., Godfrey-Smith, D.I., Thewalt, M.L.W. (1985). Optical dating of sediments. Nature 313: 105–107.

Hütt, G., I. Jaek, and J. Tchonka (1988). Optical dating: K-Feldspars optical response stimulation spectra. Quaternary Science Reviews 7: 381–385.

Kadereit, A., Kühn, P., Wagner, G.A. (2010). Holocene relief and soil changes in loess-covered areas of south-western Germany: The pedosedimentary archives of Bretten-Bauerbach (Kraichgau). Quaternary International 222: 96–119.

Markey, B.G., Bøtter-Jensen, L., Duller, G.A.T. (1997). A new flexible system for measuring thermally and optically stimulated luminescence. Radiation Measurements 27: 83–89.

Murray, A.S., Wintle, A.G. (2000). Luminescence dating of quartz using an improved single-aliquot regenerative-dose protocol. Radiation Measurements 32: 57–73.

Spooner, N.A. (1994). The anomalous fading of infrared-stimulated luminescence from feldspar. Radiation Measurements 23: 625–632.

Thomsen, K.J., Bøtter-Jensen, L., Denby, P.M., Moska, P., Murray, A.S. (2006). Developments in luminescence measurement techniques. Radiation Measurements 41: 768–773.

Visocekas, R. (1985). Tunnelling radiative recombination in Labradorite: its association with anomalous fading of thermoluminescence. Nuclear Tracks And Radiation Measurements 10: 521–529.

Wintle, A.G. (1973). Anomalous fading of thermoluminescence in mineral samples. Nature 245: 143–144.

Reviewer
R. Bailey

Reviewer's comment
As the equipment for measuring OSL becomes increasingly sophisticated, reliable, and also easier to use, the user arguably becomes more removed from the process of measurement. It is easy to forget the details of what is happening inside the equipment and to ignore the potential for systematic effects. The careful analysis described in this paper aids both the users and the designers of automated equipment in our shared goal of reducing systematic effects where we find them and improving the reliability of our results. Other aspects of the dating process will no doubt benefit from similar investigation.

A practical guide to the R package Luminescence

Michael Dietze[1,*], Sebastian Kreutzer[2], Margret C. Fuchs[3], Christoph Burow[4], Manfred Fischer[5], Christoph Schmidt[5]

[1]Institute of Geography, TU Dresden, 01069 Dresden, Germany
[2]Department of Geography, Justus-Liebig-University Giessen, 35390 Giessen, Germany
[3]Department of Geology, TU Bergakademie Freiberg, 09599 Freiberg, Germany
[4]Institute for Geography, University of Cologne, 50923 Cologne, Germany
[5]Geographical Institute, Geomorphology, University of Bayreuth, 95440 Bayreuth, Germany

* corresponding author: micha.dietze@mailbox.tu-dresden.de

_____

Abstract

A practical guide for the **R** package 'Luminescence' is provided. An introduction on data types in **R** is given first, followed by a guideline on how to import, analyse and visualise typical SAR-OSL measurement data.

Keywords: R, luminescence dating, data analysis, plotting

Introduction

Since the **R** package 'Luminescence' has been introduced by Kreutzer et al. (2012) the developer team is continuously asked for advice from the luminescence dating community. Such requests considerably help us to further improve the package and make the tools more efficient and user friendly. However, most of these queries are not directed to specific problems of the provided functions but rather on the usage of **R** and the package in general. Motivated by an e-mail conversation with Geoff Duller this contribution aims to provide an example-based, short practical guide to **R** and the package 'Luminescence'. First, we focus on properties and ways to index different sorts of data structures, which are essential for an efficient use of the **R** package 'Luminescence'. A second section describes processing steps for luminescence data, from importing a BIN-file to plotting a D_e distribution. A third section comprises the examples in a comprehensive code section.

Throughout the manuscript **R** calls or **R** related code snippets are typed in `monospaced letters`. In some cases, numerical and graphical output was truncated for illustrative reasons.

Working with R and RStudio

R (R Development Core Team, 2013) is a freely available language and environment for statistical computing and graphics. RStudio (RStudio, 2013) is a free and open source integrated development environment (IDE) for **R**. It allows for a comfortable use of **R**.

Working with **R** usually means writing of scripts that can be executed to generate results. The fundamental advantage of working with scripts rather than clicking through graphical user interfaces or tabular calculation software is that all processed steps are formulated explicitly, i.e. every command or function call is and has to be written down. This guaranties transparent and reproducible results, easy sharing of analysis routines and flexible modification of existing approaches.

A script is a text document composed of several lines of commands, and of course explanatory comments, that can be executed by software, such as **R**. Script-based execution of command line series is much more efficient than typing of function calls into the terminal window (although this is possible).

RStudio is a comfortable "second skin" to work with **R** even more conveniently. It comprises several windows; for scripts, the command line, the workspace, plot outputs, help or a file manager. RStudio allows storing entire sessions, including the actual script and generated objects (e.g. data sets and plots), to continue working at any time.

There are a series of excellent tutorials and books about **R** (e.g. Adler, 2012; Crawley, 2012) and RStudio (e.g. Verzani, 2011) that cannot be discussed here. However, on the official website of the **R** package 'Luminescence' (http://www.r-luminescence.de) there are plenty of suggestions and
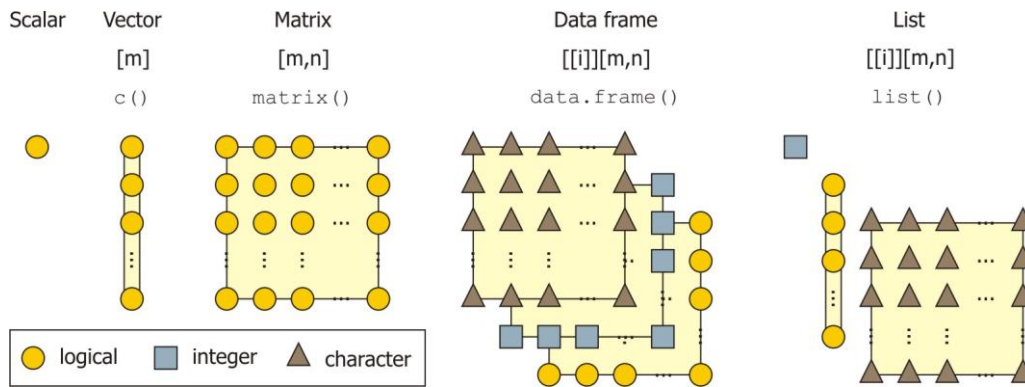
Figure 1. *Data structures in* **R***, commonly used in the package 'Luminescence'. The colour and the shape of individual objects indicate similar data types (e.g. logical, integer, character) whereas their alignment represents the structure. Code under each structure definition corresponds to the creation of the structures in* **R***. From left to right structures increase in complexity: scalar, vector, matrix, data frame, list. For further data structures and information cf. Crawley (2012).*

some tutorials dedicated to the use of **R** for luminescence data analysis.

Data types and structures in R

Data can be of various type. Common data types are logical (i.e. TRUE, FALSE), integer (e.g. 1, 2), double (e.g. 1.2, 2.3), complex (e.g. 2+3i, 1.3+3.2i) and character (e.g. "a", "b"). There are more data types in **R** but these are of minor relevance here. The type of data determines which operations are possible (or meaningful) with this data. To infer the data type of a variable use the function typeof().

Regardless of their type, data always shows a certain structure, which defines how values are organised and may be addressed. For convenient usage data may be stored in variables (or more generally in objects). It is of crucial importance to note that one variable must not necessarily comprise only one but can contain millions of individual values. **R** allows for checking the data structure of a variable with the function str(). To actually work with the data, it is necessary to "recall" the content of a variable, or parts of it. This is referred to as indexing. The following structures are commonly encountered when working with **R** and should therefore be introduced here. Fig. 1 shows illustrative sketches of the data structures.

Scalars: Scalars are the most simple data structure. One variable represents precisely one value (1,1 structure). Scalars can therefore be described as zero-dimensional data structures. In **R**, scalars are in fact vectors of length one. The command x <- 1

assigns the value 1 to the variable x. A scalar is indexed simply by calling the variable name.

Vectors: Vectors are different from scalars in that they comprise more than one value. They contain *m* rows of values, organised in one column (*m*,1 structure). Hence, vectors can be described as one-dimensional data structures. Vectors may contain any data type but this must be consistent throughout. To infer the number of elements, the length of a vector, use the function length(). To index an element of a vector, its position in the vector must be specified in angular brackets after the variable name: x[m]. To index more than one element use either a sequence (x[1:5]) or a concatenation of values (x[c(1, 2, 3, 4, 5)]).

Matrices: Adding a further dimension yields a matrix structure. Matrices contain *m* rows and *n* columns of data (*m,n* structure). Hence, matrices can be described as two-dimensional data structures. Matrices can be of any, consistent data type. Indexing matrix elements requires row- and column-numbers of the target elements in angular brackets: X[m,n]. To index an entire row or column, just skip the respective index value: X[1,] or X[,1].

Data frames: Data frames consist of components with the same geometry (same length of vectors or matrix rows and columns) but may contain different data types. Data frames are the most common data structure in **R**, as many functions require data frames as input arguments. Indexing elements of a data frame is a two-step task. First, the component and then the element of the respective component must be

indexed. The component is expressed by two nested angular brackets (`[[ ]]`). So indexing one element of a vector in a data frame may be similar to `dataframe[[1]][8]`.

Alternatively, the components of a data frame can be named. If names are present, the operator `$` can be used for indexing as well. For example, if there is a data frame (`dataframe`) comprising two vectors (`data` and `metadata`), one may index the first element of `metadata` by typing:

`dataframe$metadata[1]`

or

`dataframe[[2]][1]`.

Lists: Similar to data frames, but also deregulating the constraint of consistent geometry and data types, lists allow handling different types and structures of data. Lists are therefore the most flexible - but not necessarily the most appropriate - data structure. Indexing follows the same rules as for data frames.

S4-objects: S4 objects are of fundamentally different data structure. They are related to object-oriented programming but may be tentatively compared to lists. They can contain several components, stored in so called slots. Details on S4-objects may be not relevant in this context. Components of S4-objects are indexed by the operator `@`. Apart from this difference, indexing is quite similar to that of data frames. Note: Although the **R** package 'Luminescence' already utilises S4-objects (e.g. `Risoe.BINfileData-class`) and the upcoming package version later this year will considerably benefit from the usage of S4-objects, details on S4-objects are not relevant for this tutorial.

From BIN-files to D_e-distributions

Prerequisites for analysing luminescence data
To work with the **R** package 'Luminescence' it is first of all necessary to install the package from CRAN; either via command line (`install.packages("Luminescence", dependencies = TRUE)`) or in RStudio via menu Tools > Install Packages. Note that the checkbox "Install dependencies" should be selected. To actually use the functionalities of the package, it must be loaded at the beginning of each **R** session. Furthermore the working directory should be set. It is good practice to load the library (i.e. the functions part of a package) and define the working directory at the beginning of a script.

```
> ## load the library
> library("Luminescence")

> ## set the working directory
> setwd("/analysis/project_0815")
```

Import and inspect BIN-files
In general, analysis of luminescence data will start with importing a BIN-file to the **R** workspace. The package provides the function `readBIN2R()` to import BIN-files from typical luminescence measurements. It creates an S4-object with two slots: `METADATA` (a data frame) and `DATA` (a list). `METADATA` contains meta-information for all measurements and is primarily used to select measurements (stored in `DATA`) based on e.g. sample position. Once imported, calling the variable displays a short summary of the object.

```
> ## import the BIN-file
> SAR.data <-
+ readBIN2R("example.BIN")

> ## show a short summary
> SAR.data

> Risoe.BINfileData Object
>  Version:         03
>  Object Date:     060120
>  User:            krb
>  System ID:       30
>  Overall Records: 600
>  Records Type:    IRSL  (n = 20)
                    OSL   (n = 340)
                    TL    (n = 220)
>  Position Range:  1 : 20
>  Run Range:       1 : 44
>  Set Range:       1 : 2
```

The example data set (example.BIN) resulted from a standard SAR protocol, applied to a sample of fluvial quartz (coarse grains, 90-160 μm) from the Pamir Plateau, analysed at TU Bergakademie Freiberg in 2013, and can be downloaded from the Ancient TL website. To create a more elaborated overview, the data frame `METADATA` must be indexed by specifying the desired columns. To show, as an example, the parameters ID (1), SEL (2), LTYPE (7), POSITION (17), RUN (18), DTYPE (23) and IRR_TIME (24) for the first five measurements, the respective column-numbers must be known (see below). In practice this includes indexing the slot `METADATA` of the S4-object `SAR.data` and then indexing the first five rows and respective columns therein:

```
> SAR.data@METADATA[1:5, c(1, 2, 7,
+ 17, 18, 23, 24)]
>   ID  SEL LTYPE POSITION RUN
+ DTYPE IRR_TIME
> 1 1 TRUE  TL   1 1 Natural      0
> 2 2 TRUE OSL   1 2 Natural      0
> 3 3 TRUE  TL   1 4 Natural      0
> 4 4 TRUE OSL   1 5 Bleach+dose 80
> 5 5 TRUE  TL   1 7 Bleach+dose 0
```

If this summary content is used frequently, it may be useful to store the column-numbers in a separate variable (summary.01 <- c(1, 2, 7, 17, 18, 23, 24)) for convenient use later on (SAR.data@METADATA[,summary.01]). This way, different summary templates can be created. A complete list of column-numbers can be displayed by cbind(1:length(SAR.data@METADATA), colnames(SAR.data@METADATA)).

Analyse SAR-data

Currently, the package is focused on the analysis of measurements following the SAR protocol (Murray & Wintle, 2000). The function Analyse_SAR.OSLdata() returns a set of parameters from individual measurement cycles in order to determine background- and sensitivity-corrected signals that may be used for growth curve estimation (see below). The function requires information about the sample (i.e. position) to be analysed, the signal integral and the background integral, along with a sample ID. By default the function Analyse_SAR.OSLdata() creates a graphical output for visual inspection of measurement curves (one composite plot for each position). However, for further analysis the numeric output is more important. The following example shows how to set the necessary parameters, perform an SAR analysis and what the numerical output looks like.

```
> ## define analysis parameters
> signal <- 1:5
> backgrd <- 200:250
> position <- 1:2
> info <- "Arbitrary sample 1"

> ## analyse position 1 to 2
> SAR.results <-
+ Analyse_SAR.OSLdata(
+   input.data = SAR.data,
+   signal.integral = signal,
+   background.integral = backgrd,
+   position = position,
+   info.measurement = info)

> ## display the output
> str(SAR.results)
```

The created object (SAR.results) is a list with three components: LnLxTnTx, Rejection Criteria and SARParameters, each of them composed of further objects. To access them, just move through the data structure step by step. For example if you are interested in the second cut heat temperature type SAR.results$SARParameters$cutheat[2]. Most important (and most complex) is the LnLxTnTx-list. Since two positions were analysed (position <- 1:2) the list contains two data frames. Each data frame consists of the number of measurements according to the applied SAR protocol. Each measurement yielded 15 parameters (such as Name, Dose, Repeated, LnLx and so on). To access the LnLx data from measurement 1 (natural dose) of position 1 type SAR.results$LnLxTnTx[[1]]$LxTx[1].

Create growth curves and estimate D_e-values

From the large output amount of Analyse_SAR.OSLdata() the most important data sets for subsequent analyses are Dose, LxTx, LxTx.Error and TnTx. To create growth curves and estimate equivalent doses, these are needed in a data frame structure. The following code shows how to manage these steps.

```
> ## create data frame
> data.LxTx <- as.data.frame(cbind(
+   SAR.results$LnLxTnTx[[1]][2],
+   SAR.results$LnLxTnTx[[1]][12],
+   SAR.results$LnLxTnTx[[1]][13],
+   SAR.results$LnLxTnTx[[1]][6]))

> ## show the results
> data.LxTx

>   Dose        LxTx LxTx.Error TnTx
> 1    0   5.8947468 0.28838345 1862
> 2 1000   5.3317223 0.32684141 2006
> 3 1800   7.8098997 0.36604484 2239
> 4 2200   9.5146256 0.47587953 2393
> 5 3000  10.4157443 0.60718256 2891
> 6    0   0.5314526 0.07193097 2045
> 7 1800   7.1563381 0.46570722 2829
```

The function plot_GrowthCurve() creates a dose response curve from the measurement data. The uncertainty related to equivalent dose estimation is based on Monte Carlo simulations. The function returns the actual D_e-value, its associated error and the fit object.

```
> ## create dose response curve
> growth.curve <- plot_GrowthCurve(
+   data.LxTx)
```

```
> ## show fit parameters
> growth.curve$Fit

> ## assign De and De.error
> De.data <- cbind(
+   growth.curve$De[1:2])
```

For routine analysis it may be convenient to run this D_e modelling process in a loop for all samples of a data set.

```
> ## define analysis parameters
> signal <- 1:5
> backgrd <- 200:250
> position <- 1:20

> ## analyse positions 1 to 20
> SAR.results <-
+ Analyse_SAR.OSLdata(
+   input.data = SAR.data,
+   signal.integral = signal,
+   background.integral = backgrd,
+   position = position)

> ## Define output variable
> De.data <- data.frame(
+   De = NA,
+   De.Error = NA)

> ## Compute De values in a loop
> for(i in 1:max(position)) {
+   data.LxTx <- as.data.frame(
+     cbind(SAR.results[[1]][[i]]
+     [c(2, 12, 13, 6)]))
+   curve <- plot_GrowthCurve(
+     data.LxTx)

> ## assign De value and De error
>   De.data[i,] <- as.numeric(
+     curve$De[1:2])
+ }
```

Convert seconds to Gray

To convert the absorbed dose from seconds to the SI unit Gray the function `Second2Gray()` can be used. It includes error propagation, by default with the Gaussian approach.

```
> De.data <- Second2Gray(
+   values = De.data,
+   dose_rate = c(0.0881, 0.0006),
+   method = "gaussian")
```

Display D_e-values

There are several methods to visualise D_e distributions. Perhaps the most common ones are histograms, probability density functions based on kernel density estimates (KDE) and the radial plot (Galbraith, 1988). The chapter above illustrated how to obtain numeric data for plot outputs. One mandatory preparation step is to remove missing values (`NA`) from the `De` and `De.Error` data. This is easily done with `De.data <- De.data[complete.cases(De.data),]`.

A histogram with standard error overlay, rugs and statistical summary (Fig. 2A) can be created with the function `plot_Histogram()`.

```
> plot_Histogram(
+   values = De.data,
+   summary = c("n", "mean",
+     "median", "kdemax", "sdrel",
+     "sdabs", "serel", "seabs"))
```

Plotting a probability density plot (Fig. 2B) can be done with the function `plot_KDE()`. Further statistical summary data can be added. The following example shows most of these statistical parameters. It is left to the user to decide which parameters allow for a meaningful interpretation.

```
> plot_KDE(
+   values = De.data,
+   distribution.parameters =
+    c("mean", "median", "kdemax"),
+   summary = c("n", "mean",
+     "median", "kdemax", "sdrel",
+     "sdabs", "serel", "seabs"),
+   xlim = c(0, 450))
```

A radial plot (Fig. 2C) is created with the function `plot_RadialPlot()`. This function also supports grouped data plots, if a list with group indices is provided. For example, to plot values < 130 Gy as one group and values >= 130 Gy as a second group, the following code is needed:

```
> group.indices <- list(
+   which(De.data[,1] < 130),
+   which(De.data[,1] >= 130))
> plot_RadialPlot(
+   sample = De.data,
+   zscale.log = TRUE,
+   sample.groups = group.indices)
```
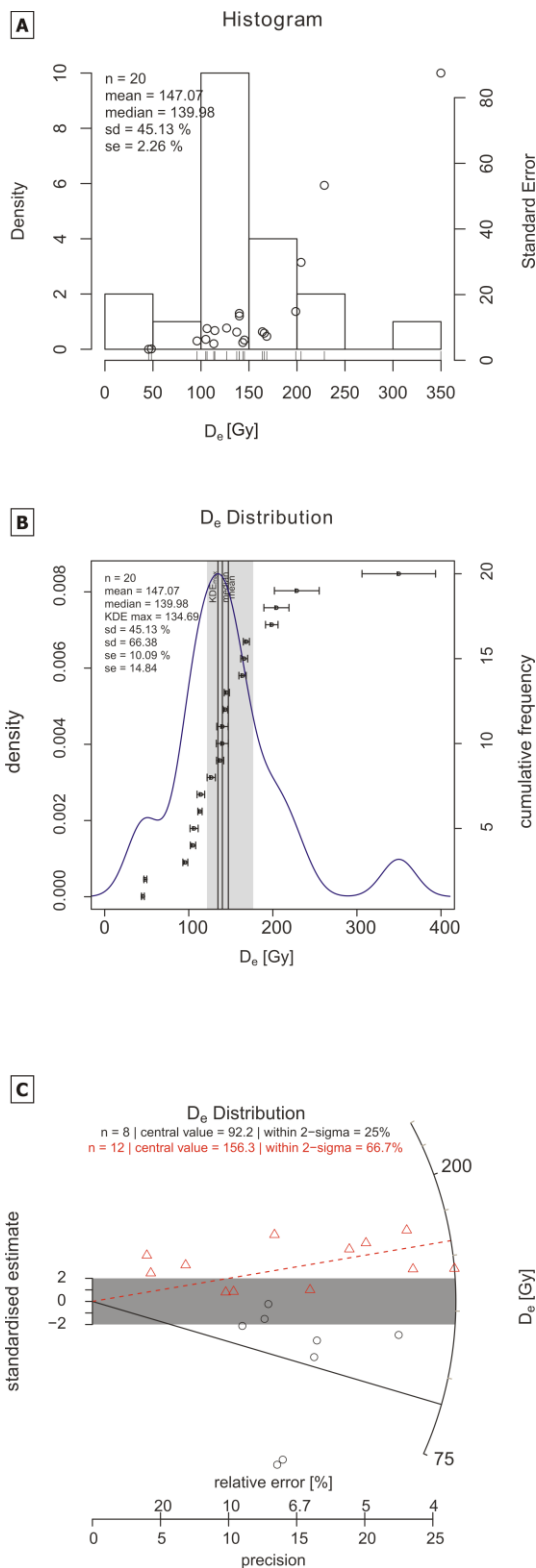
Figure 2: *Examples of plot outputs. A: histogram with rugs, standard errors and statistical measures, B: KDE-based probability density function with statistical measures, C: radial plot of grouped values.*

Save the data

  R saves data in a binary format (`*.Rdata`) with the function `save()`. To save tabular data as ASCII-files use the function `write.table()`. Re-reading data is performed by `read()` or `read.table()`.

```
> ## save R-internal data
> save(SAR.data, SAR.results,
+   De.data, file =  "SAR.RData")

> ## save De data as ASCII-file
> write.table(x = De.data, file =
+ "De_data.txt", row.names = FALSE)

> ## re-read the ASCII-FILE
> De.data <- read.table(
+   "De_data.txt", header = TRUE)
```

Export graphical output

  Saving graphical output when working with RStudio is quite easy. There is an export-button in the plots-window that allows for choosing from different formats and resolutions. However, it is also possible to export a plot directly using **R** commands. **R** can plot graphics to at least the following devices: `bmp()`, `jpeg()`, `png()`, `tiff()`, `pdf()`, `postscript()`, `win.metafile()`. Depending on the device, there are additional arguments such as `filename`, `width`, `height`, `pointsize`, `res`. Unless one wants to create further file output, it is important to close the respective device after a plot has been created. This is done by the function `dev.off()`. The function `graphics.off()` closes all open devices. To save for example a radial plot as jpg-file of 2000 by 2000 pixels with a resolution of 300 dpi the following code is needed:

```
> ## open the graphics device jpeg
> jpeg(
+   filename = "radial_plot.jpg",
+   width = 2000,
+   height = 2000,
+   res = 300)

> ## generate the plot output
> plot_RadialPlot(De.data,
+   zscale.log = TRUE,
+   zlab = expression(paste(D[e],
+     " [s]")),
+   sample.groups = group.indices,
+   sample.col = c("royalblue",
+     "orange3"),
+   sample.pch = c(3, 4),
+   cex.global = 0.9)

## close the graphics device
> dev.off()
```

```
## load the library
library("Luminescence")

## set the working directory
setwd("/analysis/project_0815")

## definition of analysis parameters
signal.integral <- 1:5
background.integral <- 200:250
position <- 1:20

## import the BIN-file
SAR.data <- readBIN2R("example.BIN")

## analyse the dataset
SAR.results <- Analyse_SAR.OSLdata(
  input.data = SAR.data,
  signal.integral = signal.integral,
  background.integral = background.integral,
  position = position)

## extract LxTx data and create De-values
De.data <- data.frame(De = NA, De.Error = NA)
for(i in 1:max(position)) {
  data.LxTx <- as.data.frame(
  cbind(SAR.results[[1]][[i]][c(2, 12, 13, 6)]))
  growth.curve <- plot_GrowthCurve(data.LxTx)

  ## extract and show De-value and delta De
  De.data[i,] <- as.numeric(growth.curve$De[1:2])
}

## convert seconds to Gray
De.data <- Second2Gray(
  values = De.data,
  dose_rate = c(0.08812, 0.00059),
  method = "gaussian")

## show the resulting matrix
De.data
```

Table 1: *Comprehensive script for routine SAR-OSL analysis*

A comprehensive script for routine SAR-OSL analysis

The code in Table 1 is a condensed, modified version of the explanations from above. It may serve as a skeleton for readers own scripts. The user is strongly advised to thoroughly inspect all graphical and numerical output to check data consistency and measurement appropriateness. An electronic version of the entire **R** script, and the example data set used in the analyses shown here, are provided as supplements to this paper and can be found at http://www.aber.ac.uk/ancient-tl.

Summary

A practical guide for the **R** package 'Luminescence' has been provided showing the steps from importing a BIN-file to plotting a D_e distribution. Further reading, including extensive examples and detailed definitions can be found on http://www.r-luminescence.de. For further suggestions and questions the package developer team can be contacted via team@r-luminescence.de.

References

Crawley, M.J. (2012). The R Book. pp. 1080, Wiley.

Galbraith, R.F. (1988). Graphical Display of Estimates Having Differing Standard Errors. Technometrics 30: 271–281.

Kreutzer, S., Schmidt, C., Fuchs, M.C., Dietze, M., Fischer, M., Fuchs, M. (2012). Introducing an R package for luminescence dating analysis. Ancient TL 30: 1–8.

Murray, A.S., Wintle, A.G. (2000). Luminescence dating of quartz using an improved single-aliquot regenerative-dose protocol. Radiation Measurements 32: 57–73.

R Development Core Team (2013). R: A Language and Environment for Statistical Computing. http://ww.r-project.org

RStudio (2013). RStudio: Integrated development environment for R (Version 0.97.449) [Computer software]. Boston, MA. Retrieved May 09, 2013.Available from http://www.rstudio.org/

Verzani, J. (2011). Getting Started with RStudio: An Integrated Development Environment for R. pp. 92. Sebastopol, CA USA.

Reviewer

G.A.T. Duller

Reviewer's Comment

I am very grateful to the authors for putting this together. The Luminescence package that they have developed for **R** has enormous potential, and hopefully this article will encourage those who are less familiar with **R** to start to use it.

Methods to reduce sample carrier contamination for luminescence measurements

Lauren Miller Simkins[1]*, Regina DeWitt[2], Alexander Simms[1]

[1]Department of Earth Sciences, University of California-Santa Barbara
[2]Department of Physics, East Carolina University

* Corresponding author: lauren.m.simkins@gmail.com

_____

Abstract

Equivalent doses derived from sediment measurements void of signal contamination are essential for accurate optically stimulated luminescence (OSL) dating of sediments. We identified dose-dependent luminescence signals originating from new and previously used stainless steel cups used for OSL measurements. The signal is not eliminated under typical measurement conditions for sedimentary quartz including pre-heating, infrared stimulation, and OSL stimulation at 125°C. While signals from sample carriers are typically small sources of error they may strongly contaminate sediment with low OSL sensitivities. We tested several cleaning methods on used and new stainless steel cups by measuring OSL signals after increasing irradiation doses between 0 and 100 Gy. The lowest signal from sample carriers was observed from cleaning with HF, Alconox (a detergent for silicone oil removal), and methanol. The cleaning methods that produce the lowest signal from the cups were combined to create two modified cleaning procedures that are effective in reducing the unwanted luminescence signal. Our newly modified cleaning methods are capable of reducing the luminescence signal of empty stainless steel cups to near background levels.

Introduction

Unwanted signal contributions can lead to the miscalculation of equivalent doses used for optically stimulated luminescence (OSL) ages. Recent studies have identified luminescence signals from sample carriers (Schmidt et al., 2011) and silicone oil (Vandenberghe et al., 2008) used for OSL measurements. Unlike sensitivity changes and background measurements, variable signal contamination produced by sample carriers is not accounted for in the single aliquot regenerative (SAR; Murray and Wintle, 2000) dose measurement

procedure thus sample carriers pose as a source of error for sediment measurements.

Typical sample carriers used for OSL dating include stainless steel and aluminum discs and cups. Schmidt et al. (2011) observed significant dose-dependent thermal luminescence (TL) signals from clean, empty stainless steel and aluminum discs with strong TL peaks at 110 °C in ultraviolet (UV; 340 nm) and UV-blue (420 nm) detection windows. Two other peaks were observed between 150 and 300 °C in the UV range and a broad peak was observed between 150 and 300 °C in the UV-blue window with a high-temperature peak at 380 °C. Additionally, Vandenberghe (pers. comm.) identified ultra-fast decaying, thermally unstable, dose-dependent signals from stainless steel discs with a strong TL peak at 110°C with a UV (340 nm) detection window. Luminescence signals from empty sample carriers most likely arise from chemical reactions between silicone oil and sample carriers upon heating and irradiation that result in luminophores derived from defects in silica-, aluminum-, and iron-oxides (Schmidt et al., 2011). Since sample carriers are generally recycled from measurement to measurement, the luminescent film may build up with increased usage due to its impervious nature to cleaning.

Typically small sources of error have a relatively large influence on sediments with low OSL sensitivities. The goal of this study is to explore sample carriers as a possible source of contamination and devise an effective cleaning procedure in order to minimize equivalent dose distribution scatter. After determining the magnitude of contaminant signals from sample carriers, we test empty stainless steel cups under measurement conditions typically used for sedimentary quartz. Multiple cleaning methods were conducted on stainless steel cups to eliminate contaminant signals. We established modified cleaning procedures for stainless steel cups based on

the cleaning methods that produced the lowest and least variable contaminant signals. We investigate the effectiveness of our newly modified cleaning techniques by measuring equivalent doses of two Antarctic cobble surfaces with low OSL sensitivities using sample carriers cleaned prior to and after the adoption of our modified cleaning procedures.

Methods

Measurements for this study were conducted at the Radiation Dosimetry Laboratory at Oklahoma State University using a Risø TL/OSL-DA-15 Reader manufactured by Risø National Laboratory including a built-in ^{90}Sr/^{90}Y beta source with an internal dose rate of 100 mGy s^{-1}, and measuring OSL with blue LEDs (470 nm, 31 mW cm^{-2}), infrared stimulated luminescence (IRSL) with an IR LED array (~875 nm, 110 mW cm^{-2}), and detection in the UV band (Hoya U340, 7.5 mm, 340 nm peak; Bøtter-Jensen and Murray, 1999). A heating rate of 5°C s^{-1} in a N$_2$-atmosphere was used for measurement stimulation above room temperature.

Luminescence signals from sample carriers
Measurement sequence

We used stainless steel cups as sample carriers provided by Risø DTU with a diameter of 9.8 mm and thickness of 0.5 mm. Raw material for the cups is PK11NB stainless steel (Mat.No. 1.4550, DIN X6CrNiNb18-10, AISI 347) from Metal Ravne (www.metalravne.com; H. Christiansen, pers. comm.). The cups have been recycled for several years and cleaned between measurements with our standard cleaning method (termed "Ethanol" in Appendix I in the supplementary information) comprised of two 30-minute ultrasonic baths with de-ionized (DI) water and dish soap followed by individual cleaning with ethanol. We visually inspect each cup to insure all grains were removed during cleaning. All measurements on empty cups conducted in this study were not sprayed with silicone oil.

Nine cups were initially tested to determine whether empty stainless steel cups have contaminant signals by measuring OSL at room temperature and 125°C for 100 s. Each data channel during OSL measurement represents the signal emitted in 0.4 s. Further measurements were conducted on the same cups to observe the characteristics of contaminant signals under measurement conditions used for sedimentary quartz. After irradiation of 100 Gy, signals from empty cups were measured using OSL at room temperature and 125°C for 40 s. We recorded TL curves for the cups during pre-heating to 200°C followed by measurement of OSL (125°C, 40 s). IR stimulation is commonly used in SAR measurement sequences to bleach contaminant

feldspars (Wallinga, 2002; Duller, 2003; Wintle and Murray, 2006) thus we test: (1) whether the cups have signal when exposed to IR stimulation (60°C, 100 s); and (2) how the signal changes when IR stimulation (60°C, 100 s) is used prior to OSL measurement (125°C, 40s).

Measurements on the same nine cups were conducted with quartz (90-212 μm) extracted from an Antarctic beach cobble surface (sample CB10-059; Simkins et al., in review). Quartz grains (n=100-200) were adhered to the cups using silicone oil and the entire cup area was covered with a monolayer of quartz. To test whether contaminant OSL signals arise during sediment measurements, we irradiated empty cups with 100 Gy then covered the cups with bleached quartz. We bleached the quartz by pre-heating at 200°C for 60 s followed by IR stimulation at 60°C for 100 s and measurement of OSL at 125°C for 200 s. OSL signals of the irradiated cups with bleached sediment cover were measured at 125°C for 40 s following pre-heating (200°C, 10 s) and IR (60°C, 100 s) stimulation. Lastly, the cups and quartz were irradiated simultaneously with 100 Gy and OSL signals were measured following the same sequence as with bleached quartz.

Results

Stainless steel cups do not produce OSL signals in the absence of prior irradiation when measured at 125°C or room temperature (not shown) following cleaning with the standard cleaning method (Appendix I). After irradiation of 100 Gy, the decay curves have fast components with background signals established by the first second of stimulation at both room temperature and 125°C (Fig. 1a). Measurement of OSL at room temperature produces higher signals than when measured at 125°C. TL curves recorded during pre-heating (up to 200°C) show a prominent peak centered at 100°C (Fig. 1b). OSL signals from empty cups are reduced to below 500 counts for all nine cups when pre-heating (200°C for 10 s) is used (Fig. 1c). Empty cups show no signals above background when stimulated with IR with the exception of two of the nine cups with signals 20-30 counts above background (Fig. 1d). OSL signals increase following IR stimulation (Figure 1c versus 1e). Contaminant signals from empty cups are not eliminated when pre-heated (200°C, 10 s) and stimulated by IR (60°C, 100 s) prior to OSL measurement (Fig. 1e).

A TL curve recorded during pre-heating is shown for irradiated cups with bleached quartz covering the surface of the cups (Fig. 1f) as well as for irradiated cups with irradiated quartz (Fig. 1g). The OSL curves for irradiated cups with bleached quartz (Fig. 1h)
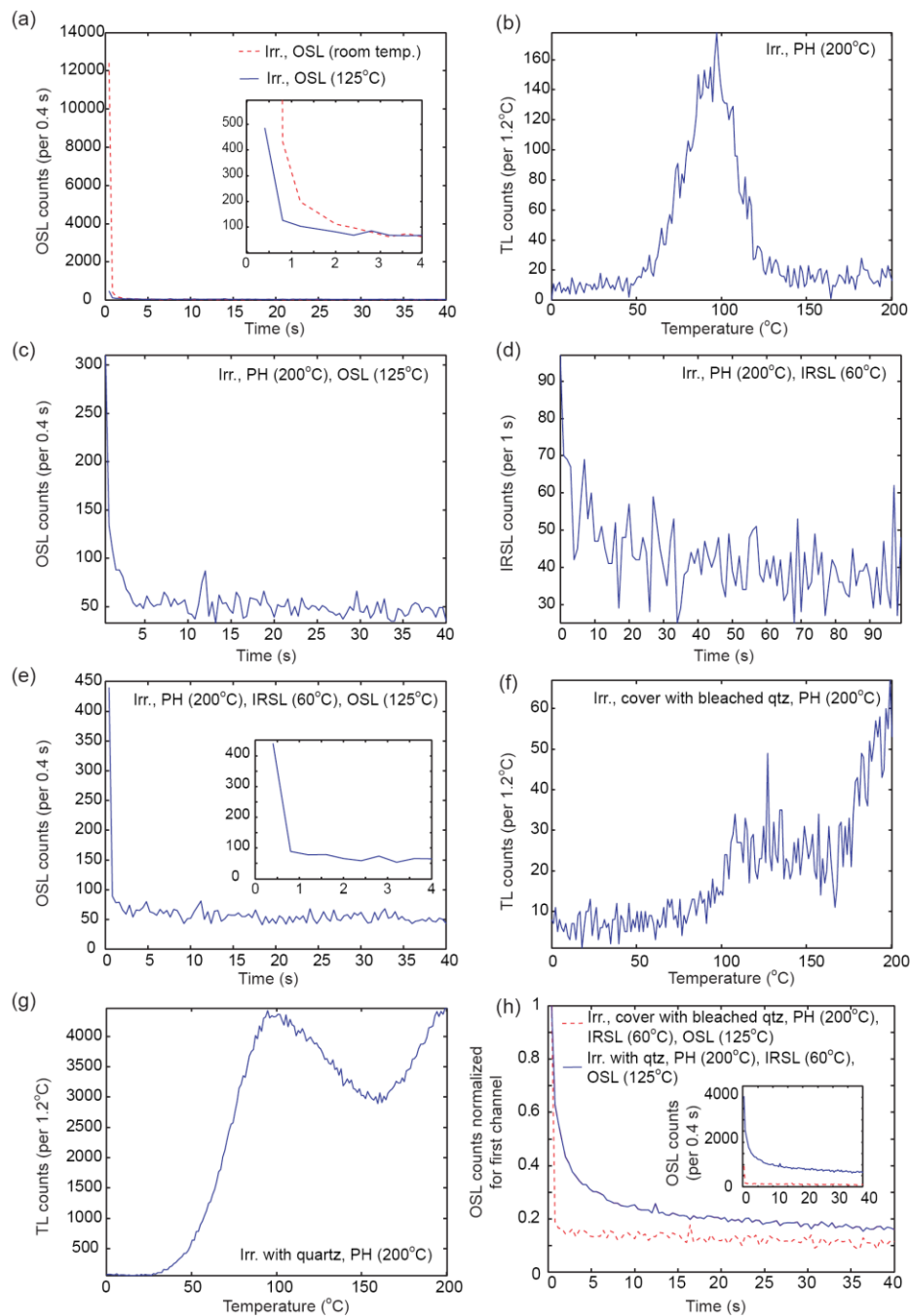
Figure 1: *Measurement of OSL signals from one representative empty cup out of the nine measured cups at (a) room temperature for 40 s (red dashed line) and 125°C for 40 s (blue line) following irradiation (irr.) of 100 Gy. (b) TL curve recorded during pre-heating (PH) to 200°C following irradiation of 100 Gy. (c) OSL curve measured at 125°C for 40 s following irradiation (100 Gy) and pre-heating (200°C, 10 s). (d) IRSL (60°C, 100 s) after irradiation (100 Gy) and pre-heating (200°C, 10 s). (e) OSL (125°C, 40 s) following irradiation (100 Gy) and pre-heat (200°C, 10 s) and IRSL (60°C, 100 s). Inset shows decay during the first 4 s of stimulation with the same y-axis as the full OSL decay curve. (f) TL curve from pre-heat (PH) (up to 200°C) using irradiated cups (100 Gy) with bleached quartz covering the cup surface. (g) TL curve recorded during pre-heat to 200°C following cup and quartz irradiation of 100 Gy. (h) Resulting OSL curves normalized for the signal in the first channel for bleached (red dashed line) and irradiated (blue line) quartz following irradiation (100 Gy), pre-heat (200°C, 10 s), and IRSL (60°C, 100 s) with an inset of the raw decay curves with the same y-axis as the normalized decay curves.*

(a)

(b)
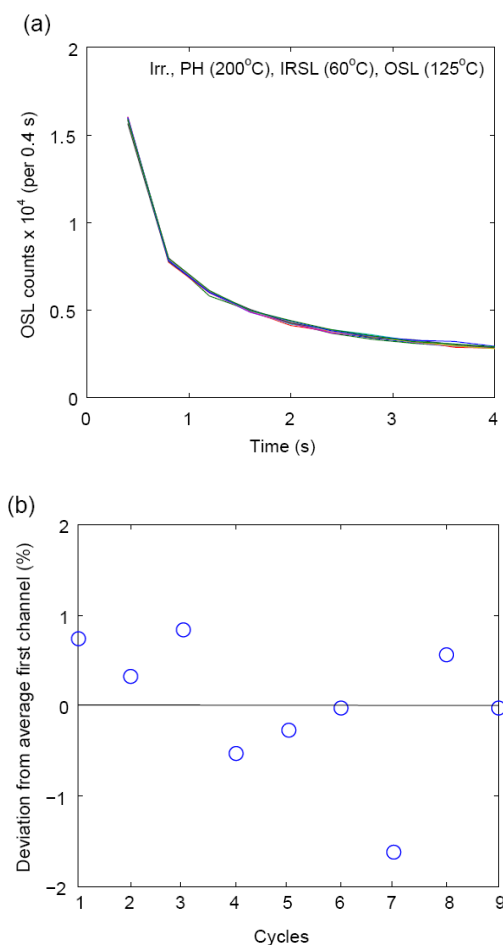
Figure 2: *(a) Decay curves for one empty stainless steel cup during the first four seconds of OSL (125°C, 40 s) for nine measurement cycles including irradiation (30 Gy), pre-heat (200°C, 10 s), and IRSL (60°C, 100 s) prior to OSL stimulation. (b) Deviation in percent from average signal in first channel for the nine measurement cycles. The line at 0 along the y-axis represents the average signal.*

shows fast decay as observed for all empty cup measurements. OSL decay curves resulting from irradiated cups with irradiated quartz (Fig. 1h) show a slower component not observed from empty cups or cups covered with bleached quartz.

Sample carrier sensitivity test
Measurement sequence

Additional measurements on one empty cup were conducted to assess whether empty cups experience sensitivity changes during measurement sequences. We used nine repeated cycles of irradiation of 30 Gy followed by pre-heat (200°C, 10 s), IR stimulation (60°C, 100 s), and OSL measurement (125°C, 40 s).

Results

OSL signals measured for the repeated cycles show less than 2 % deviation from the average OSL signal from the first channel of the nine cycles (Fig. 2). We suggest signals from stainless steel cups do not change sensitivity with repeated measurement cycles.

Cleaning procedures
Measurement sequence

Several cleaning techniques were applied to empty cups in addition to the standard cleaning method (Appendix I). Following two ultrasonic baths with dish soap and DI water, cleaning was performed with acetone, methanol, sand paper, and hydrofluoric acid (HF). In addition, Alconox (Powdered Precision Cleaner, www.alconox.com), a detergent for ultrasonic removal of silicone oils, and Rust Stain Remover (manufactured by Whink), containing approximately 3% HF, were tested as substitutes for dish soap in the ultrasonic baths. For the use of Alconox, we used an approximate mixing ratio of 10 g of Alconox per 1 liter of DI water. The ultrasonic baths with Rust Stain Remover contained 1 part Rust Stain Remover to 3 parts DI water. Each cleaning method was conducted on five randomly selected empty cups that have been previously used for sediment measurements. New (i.e. unused) cups were also tested for luminescence signals including five new cups with no cleaning treatment and five new cups cleaned with Alconox.

The higher the signal the better the resolution at which we can test the cleaning methods. For this reason, measurements of individual cleaning techniques and modified cleaning procedures were conducted with OSL stimulation at room temperature (see Fig. 1a). In order to determine the dose-dependency of the cups using various cleaning procedures, OSL signals were measured for 100 s at room temperature after irradiation of 0, 1, 10, 50, and 100 Gy. The reported signals are the sum of the first two seconds of stimulation. The slow component was removed by subtraction of the background signal (last 10 s). The cleaning methods that produced the lowest, least variable signals from the cups were combined to create modified cleaning procedures. Modified cleaning procedures were applied to the cups and tested by measuring OSL signals at room temperature for 100 s after irradiation of 100 Gy.

Results

Irrespective of the cleaning method, OSL signals were not observed for stainless steel cups that were not irradiated prior to OSL stimulation (not shown). Results from irradiated cups cleaned with various treatments are summarized in Fig. 3. Dose response curves (Appendix II) for cups cleaned with each
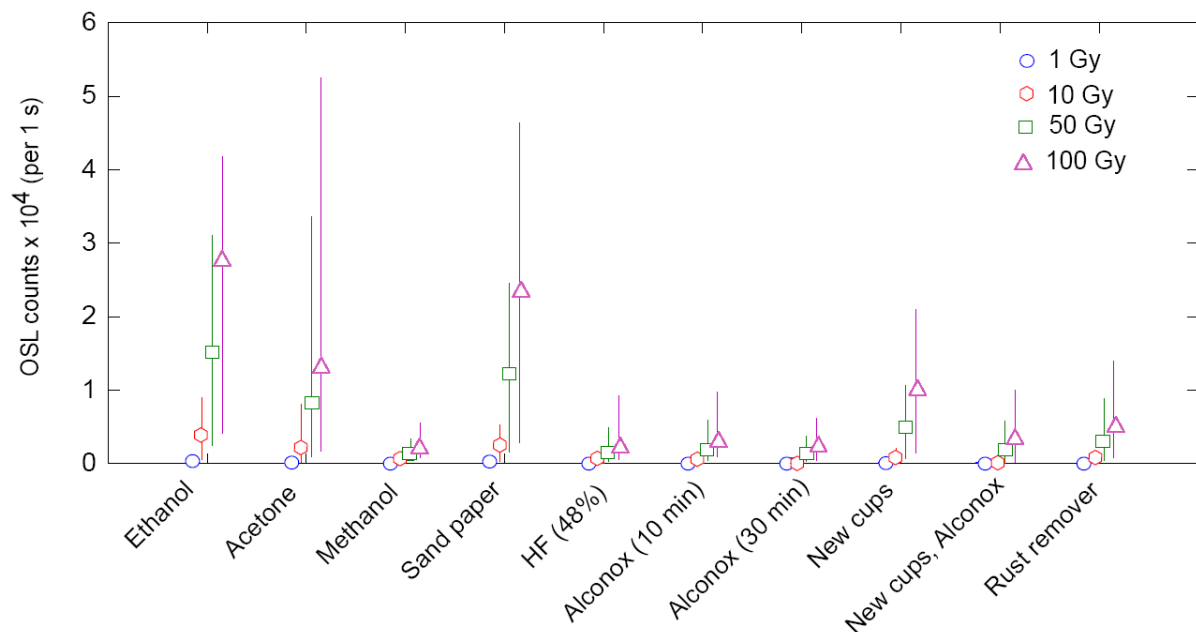
Figure 3: *OSL signals (measured at room temperature for 100 s) from five empty stainless steel cups cleaned with the cleaning methods (see Appendix I for details). The cleaning methods are listed along the x-axis. The signals include the integral from the first two channels. The error bars represent the range of signals from the five empty cups cleaned with the same method and irradiated with the same dose while the points represent the averages. OSL measurements were conducted after irradiation doses of 1, 10, 50, and 100 Gy. 1 Gy – blue circles; 10 Gy – red hexagons; 50 Gy – green squares; 100 Gy – magenta triangles.*

individual cleaning technique show, with a few exceptions, a linear trend in signal growth with increased irradiation dose. Even after 1 Gy, empty cups cleaned with ethanol, acetone, and sand paper produced luminescence signals above background (> 100 counts). After irradiation of 100 Gy, cups have OSL signals up to 53000 counts. Cleaning with ethanol (standard cleaning method), acetone, and sand paper produced the highest, most variable signals suggesting these methods are least effective in removing the luminescence signal of the cups. The use of methanol, HF (48%), Alconox, and Rust Stain Remover (3 % HF) produced the lowest and least variable OSL signals.

A combination of the most effective methods was adopted to create two modified cleaning procedures for stainless steel cups (Table 1). Method (1) consists of ultrasonic baths with Alconox, etching with 48% HF for 5 minutes, and individual scrubbing with methanol. Method (2) is similar to method (1) with the exception of using Rust Stain Remover instead of 48% HF. A total of 240 and 130 cups were cleaned with cleaning methods (1) and (2), respectively. The cleaning methods were tested on cups using irradiation of 100 Gy followed by OSL at 125°C for 100 s. The majority of cups (61%) cleaned with method (1) have OSL signals between 100-500 counts with only 2 % of the cups with signals < 100

counts. The majority of cups (89%) cleaned using method (2) have signals less than < 500 counts with a larger percentage (41%) of cups with signals below 100 counts.

Impact of contamination on equivalent doses
Measurement sequence

OSL measurements from two quartz isolates (90-212 μm; 100-200 grains) extracted from buried Antarctic cobble surfaces were measured using stainless steel cups cleaned with our standard cleaning method (Appendix I). See Simms et al. (2011) for details on sediment sample preparation. Equivalent doses were determined following the SAR measurement protocol (Murray and Wintle, 2000) using the same laboratory facilities and stimulation and detection windows mentioned in the methods section. We used a pre-heat of 200°C for 10 s, a cut-heat of 180°C for 10 s, IR stimulation at 60°C for ≤ 100 s, and OSL was measured at 125°C for 100 s. Each SAR cycle was followed by measurement of OSL at high-temperature (240°C, 10 s; Murray and Wintle, 2003). The first two channels of the OSL signal curve were used as the signal for equivalent dose calculations. The slow component of the OSL curve was removed by subtraction of the background signal (last 10 s). We consider passing aliquots to have recycling ratios < 20 %, recuperation tests with
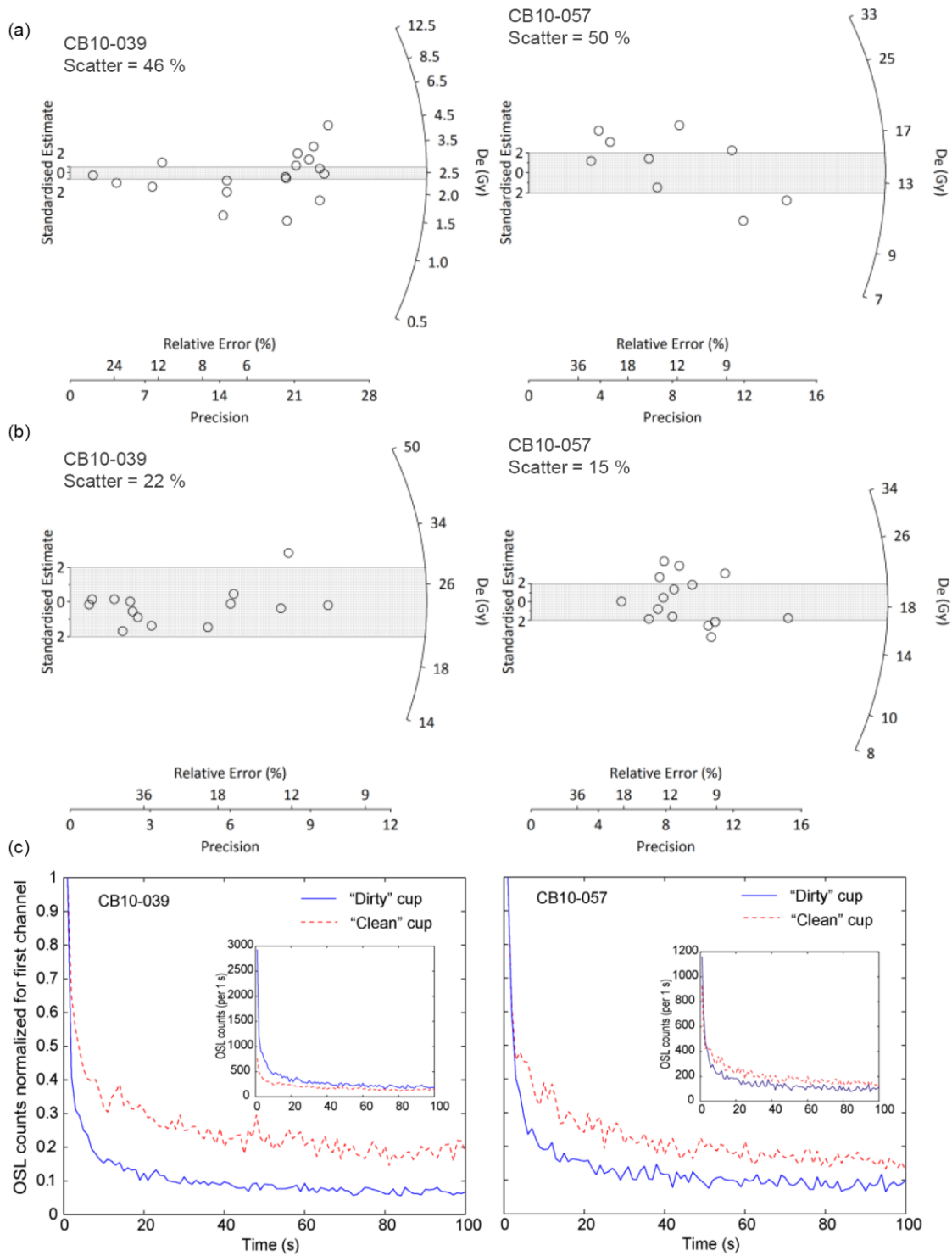
Figure 4: *(a) Radial plots showing equivalent doses distributions from two quartz samples (CB10-039 and -057) from Antarctica cobble surfaces derived from measurements made using stainless steel cups cleaned with the standard cleaning method. (b) Re-measured equivalent doses distributions from the same samples using neutral-signal cups cleaned with modified cleaning method (2). (c) OSL decay curves normalized for the signal in the first channel for samples CB10-039 and CB10-057 after irradiation of 30 and 50 Gy, respectively, using cups with contaminant signals (blue line) and neutral signals (red dashed line). The inset shows the raw OSL decay curves with the same x-axes as the normalized decay curves.*

Cleaning method (1) - Alconox, HF, and methanol

Step 1: Rinse with DI water
Step 2: 30-min. ultrasonic bath (Alconox at 70°C)
Step 3: Rinse with DI water
Step 4: Etch with 48% HF for 5 minutes
Step 5: Rinse with DI water
Step 6: 30-min. ultrasonic bath (Alconox at 70°C)
Step 7: Rinse with DI water
Step 8: Scrub each cup with methanol using a cotton swab

Cleaning method (2) - Alconox, Rust Stain Remover, and methanol

Step 1: Rinse with DI water
Step 2: 1-hr ultrasonic bath (Alconox at room temp)
Step 3: Rinse with DI water
Step 4: 1-hr ultrasonic bath (Rust Stain Remover at room temp)
Step 5: Rinse with DI water
Step 6: 1-hr ultrasonic bath (Alconox at room temp)
Step 7: Rinse with DI water
Step 8: Scrub each cup with methanol using a cotton swab

Table 1: *Modified sample carrier cleaning methods*

values < 10 %, and dose recovery ratios < 25 %. The dose recovery test differs from the dose recovery test suggested by Wintle and Murray (2006) which refers to the recovery of a dose that was administered to unheated bleached aliquots by giving a dose between regenerative cycles 2 and 3 using thermal treatments as for the regenerative cycles. Statistical modeling following the common age model (Galbraith et al., 1999) yielding a weighted log paleodose was used to determine the most representative equivalent dose from dose distributions. We tested the effectiveness of our modified cleaning methods by re-measuring equivalent doses of the same sediment samples using cups without contaminant signals. The measurement sequence for re-measured samples was identical to the sequence used for equivalent doses from measurements using contaminant-signal cups.

Results

We observe large intra-sample scatter as evidenced in radial plots of equivalent dose distributions derived from quartz extracted from buried Antarctic cobble surfaces using cups cleaned with the standard cleaning method (Fig. 4a). The scatter is quantified by dividing the standard deviation of all passing aliquots by the simple average of equivalent doses and is shown as "Scatter" in the top left of the radial plots. Dose distributions of re-measured samples

Sample	"Dirty" cups D_e (Gy)	"Clean" cups D_e (Gy)
CB10-039	2.46 ± 0.03	24 ± 1
CB10-057	13.7 ± 0.5	24.5 ± 0.5

Table 2: *Equivalent doses (D_e) of Antarctic cobble surfaces*

using cups cleaned with modified cleaning method (2) with Rust Stain Remover show the majority of aliquots plotting within two standard deviations of the equivalent dose estimate from the age model (Fig. 4b). The re-measured equivalent doses show less scatter than equivalent doses derived from measurements with cups with contaminant signals. Equivalent doses for the two samples after the adoption of our modified cleaning procedure are higher than for measurements using cups with contaminant signals (Table 2). OSL signals measured after irradiation of 30 and 50 Gy for CB10-039 and CB10-057, respectively, show faster decay curves when quartz is measured on cups with contaminant signals (Fig. 4c).

Discussion

Luminescence signals from sample carriers

We observe that both new and previously used empty stainless steel cups produce dose-dependent signals when measured at 125°C as well as at room temperature. Fig. 1 summarizes the characteristics of contaminant signals from stainless steel cups. Contaminant signals from empty cups are not eliminated by the thermal pre-treatment (pre-heat for 10s at 200°C) or the prior exposure to IR stimulation (60°C, 100 s). Covering the surface of the cups with bleached quartz does not mask the contaminant signals. On the contrary, despite ensuring the quartz used was bleached, OSL signals increase with cups covered with bleached quartz using the same sequence with pre-heat and IR stimulation (Fig. 1e and 1h). Sensitivity changes could potentially explain the higher signals; however, considering sensitivity changes are not observed for empty cups (Fig. 2), the higher signals cannot be attributed to sensitivity changes during measurement sequences. The fast nature observed from empty cups and cups covered with bleached quartz is not observed under typical sediment measurement conditions with irradiated quartz most likely due to the combination of slower OSL decay from the quartz with fast decay from the cups themselves (Fig. 1h). We show that contaminant signals from stainless steel cups used as sample carriers are: (1) impervious to our standard cleaning

methods, (2) not eliminated using typical measurement conditions for sedimentary quartz (e.g. thermal preheating, IR stimulation and elevated temperature OSL measurement; and (3) not masked by sediment covering the cups. These findings are in support of the work of Schmidt et al. (2011) who suggest the presence of contaminant signals from sample carriers.

Cleaning methods

Previously used and new cups have contaminant signals when cleaned with multiple techniques; however, signals were not observed without prior irradiation. The signals observed following various cleaning methods (Fig. 3) suggests the contaminant signal from stainless steel cups is variable and dose dependent. Considering sensitivity changes were not observed for empty cups, we attribute the growth in signal magnitude with increasing irradiation dose to the dose-dependency of the contaminant signals.

Signals produced by new stainless steel cups most likely result from silicone oil used in manufacturing of the cups. Luminescence signals from previously used cups most likely arise from reactions that take place upon heating and irradiation of previously used cups resulting in luminophores derived from defects in silica-, aluminum-, and iron-oxides (Schmidt et al., 2011). We find that our standard cleaning method does not sufficiently remove OSL signals from new and previously used cups. However, we identify the most effective cleaning methods for stainless steel cups including methanol, Alconox, HF (48 %), and Rust Stain Remover (3 % HF).

Modified cleaning procedures (Table 1) minimize luminescence signals produced by stainless steel cups. Both cleaning procedures use HF in different concentrations. HF is well known for its ability to dissolve iron- and silica- oxides and is commonly used to remove impurities from stainless steel. Of the two cleaning methods, method (2) is more effective at reducing the signal to less than 100 counts or otherwise close to background signals (Fig. 3). Additionally, although HF is present in Rust Stain Remover, cleaning method (2) eliminates the use of strong concentrations of HF.

We advise that following the first use of either modified cleaning procedure, cups should be tested for luminescence signals following irradiation of 100 Gy. Cups that produce signals above 100 counts should be discarded or re-cleaned and re-tested prior to use for equivalent dose measurement of dim quartz. However, for brighter quartz, contaminant signals from stainless steel cups > 100 counts may be acceptable. After cups are initially cleaned and used in sample measurements, we conduct routine tests on the cups after each cleaning treatment by selecting five clean cups at random to verify that the cups have signals less than 100 counts.

Impact of contamination on equivalent doses

Luminescence signals from stainless steel cups contaminate OSL measurements of sedimentary quartz (Figs. 1 & 4). Considering signals from cups are dose-dependent, natural OSL signals from sediment for dating purposes are not contaminated by sample carriers; however, the dose response curve results from a combination of signals from sediments and stainless steel cups. The resulting higher equivalent doses of sediment samples (Table 2) using cups with no signal suggest that the dose-dependent luminescence signals from stainless steel cups previously dominated the dose response curve without contributing to the natural signal from dated samples. When using cups with contaminant signals, we suggest sediment natural signals appear relatively small compared to regenerated dose responses thus equivalent dose estimates underestimate true OSL ages. Our modified cleaning methods allow for more robust sample measurements and equivalent dose estimates for Antarctic cobble surfaces with low OSL sensitivities.

Conclusions

We report variable, dose-dependent luminescence signals from new and previously used empty stainless steel cups used as sample carriers for OSL measurements. Contaminant signals are reduced but not eliminated using pre-heat (200°C, 10 s) and IR (60°C, 100 s) stimulation. Signals generated by the cups are not masked by sediment cover. The remaining contaminate signal from stainless steel cups introduce a source of error for OSL measurements of sedimentary quartz. Our standard cleaning method is not effective in removing the luminescence signal from stainless steel cups. Two modified cleaning methods combine the use of Alconox, HF (48% and 3%), and methanol in order to reduce unwanted signals from new and used stainless steel cups. After cleaning cups using our modified cleaning methods, much of the dose distribution scatter initially observed for Antarctic cobble surfaces is resolved. The application of these cleaning methods to stainless steel cups used as sample carriers reduces signal contamination of low OSL sensitivity quartz where typically small sources of error can produce relatively large measurement uncertainty. Our modified cleaning methods may potentially be useful for other applications of luminescence methods to produce more robust measurements void of unwanted contamination from sample carriers.

Supplementary information for this article is available at the Ancient TL web site (www.aber.ac.uk/ancient-tl).

References

Bøtter-Jensen, L., Murray, A.S., 1999. Developments in Optically Stimulated Luminescence Techniques for Dating and Retrospective Dosimetry. Radiation Protection Dosimetry 84: 307-315.

Duller, G.A.T., 2003. Distinguishing quartz and feldspar in single grain luminescence measurements. Radiation Measurements 37: 161-165.

Galbraith, R.F., Roberts, R.G., Laslett, G.M., Yoshida, Y., Olley, J.M., 1999. Optical dating of single and multiple grains of quartz from Jinmium rock shelter, northern Australia: part 1, experimental design and statistical models. Archaeometry 41: 339-364.

Murray, A.S., Wintle, A.G., 2000. Luminescence dating of quartz using an improved single-aliquot regenerative-dose protocol. Radiation Measurements 32: 57-73.

Murray, A.S., Wintle, A.G., 2003. The single aliquot regenerative dose protocol: potential for improvements in reliability. Radiation Measurements 37: 377-381.

Schmidt, C., Kreutzer, S., Fattahi, M., Bailey, R., Zander, A., Zöller, L., 2011. On the luminescence signals of empty sample carriers. Ancient TL 29: 65-74.

Simms, A.R., DeWitt, R., Kouremenos, P., Drewry, A.M., 2011. A new approach to reconstructing sea levels in Antarctica using optically stimulated luminescence of cobble surfaces. Quaternary Geochronology 6: 50-60.

Simkins, L.M, Simms, A.R., DeWitt R., in review. Relative sea-level history of Marguerite Bay, Antarctic Peninsula derived from optically stimulated luminescence-dated beach cobbles.

Vandenberghe, D.A.G., Jain, M., Murray, A.S., 2008. A note on spurious luminescence from silicone oil. Ancient TL 26: 29-32.

Wallinga, J., 2002. Optically stimulated luminescence dating of fluvial deposits: a review. Boreas 31: 303-322.

Wintle, A. G., Murray, A. S., 2006. A review of quartz optically stimulated luminescence characteristics and their relevance in single-aliquot regeneration dating protocols. Radiation Measurements 41: 369-391.

Reviewer
D.A.G. Vandenberghe

Editor's comment
This is the latest in a series of papers in Ancient TL dealing with unwanted signals during luminescence measurements, and they highlight the need for care. The practise of checking sample holders prior to measurement is a good one. Although the formation of phosphors by chemical reactions with the substrate of the sample carrier is a concern, in my experience the most common problem that colleagues find is that they have not completely removed all the quartz and/or feldspar from their carriers, and that it is this which may provide a problem.

Thesis Abstracts

Author: Christoph Schmidt
Thesis Title: Luminescence dating of heated silex – Potential to improve accuracy and precision and application to Paleolithic sites
Grade: Ph.D.
Date: August 2012
Supervisors: Alexandra Hilgers, Ulrich Radtke
Address: Institute for Geography, University of Cologne, Otto-Fischer-Str. 4, 50674 Köln, Germany
(Present address: Geographical Institute, Geomorphology, University of Bayreuth, 95440 Bayreuth, Germany)

Thermoluminescence (TL) dating of heated silex artefacts represents an important chronometric tool for Middle to Upper Paleolithic archeological contexts. Since the firing of these lithics can legitimately be attributed to human agency, this method provides direct age estimates of the occupation of a site. However, in relation to other dating methods, the precision of TL dates is comparatively low, and the often observed "overdispersion" in ages of obviously syndepositional finds indicates additional sources of scatter mainly disregarded so far. This thesis examines potential sources of both imprecision and inaccuracy of age estimates as well as the capability of alternative approaches to overcome or reduce these shortcomings of the TL method applied to heated silex.

Besides assessing the influence of spurious luminescence signal contributions from sample carriers on determined dose, focus is set on investigating strength and uniformity of the internal dose rate of silex samples and resulting effects on the age. Being constant over burial time, self-dosing may either decrease the influence of elusive and variable external radiation – in case of homogeneous radioelement distribution within the sample – or introduce systematic errors and enhanced data scatter, if radiation is concentrated in "hot spots". With α- and β-autoradiography and laser ablation inductively coupled plasma mass spectrometry (LA-ICP-MS), both qualitative and quantitative approaches served to draw a detailed picture on presence and spatial distribution of hot spots and associated impurities in

thick sections of over 20 silex specimens. While the low β-activity of most samples is rarely visible on respective autoradiographs, recorded α-tracks revealed zones and spots with strongly increased Th and U concentrations. Comparison of autoradiographs with sample surfaces shows a clear relationship between track density and impurities or filled cracks. These findings are confirmed by LA-ICP-MS: In contrast to the low radioactivity of pure silex, most kinds of impurities are related to strongly increased radiation. If this is not accounted for, micro-dosimetric effects may lead to random and systematic errors in age determination.

Additionally, the performance of TL single-aliquot regenerative-dose (SAR) protocols for dating small-sized samples and as a diagnostic tool for non-uniform dose distribution in the samples was tested. For both the blue (~475 nm) and red (~630 nm) TL emission it was found that the degree of adequate sensitivity-correction by test dose monitoring strongly depends on the properties of individual samples. However, laboratory doses could be well reproduced for most specimens. By comparing De distributions from natural dose measurements and dose recovery tests and regarding the value range of sensitivity corrected natural signals (L_n/T_n), assessment of sample homogeneity and SAR dose response behavior is enabled, respectively.

Unlike for commonly used TL, few is known about optically stimulated luminescence (OSL) of silex. However, access to specific, optically sensitive trap populations (e.g. slow-components) and more gentle heat treatment in the course of SAR sequences may yield the benefits of increased saturation dose levels (and hence upper dating limits) and reduced systematic errors, respectively. Therefore, fundamental properties such as signal composition and thermal long-term stability of silex OSL were studied and its applicability to heated samples evaluated. First-order fitting of linearly modulated (LM-) OSL curves showed best results for five components in most cases. Pulse annealing experiments and the varying heating rate method, however, attested only the best bleachable component sufficient thermal stability. Successful dose recovery tests and OSL ages in agreement to TL ages of the same samples validate the general applicability of this OSL component for dating. However, since not all silex varieties show an optical signal at all, this approach may be regarded as complementary to TL and reassuring for important samples.

In the applied part of this thesis, several sets of heated artefacts from Middle and Upper Paleolithic

sites in Portugal, Spain, Romania and Egypt were TL and OSL dated. Gravettian samples from Vale Boi (Portugal) were submitted for dating after termination of the excavation, so that environmental radiation could not be determined accurately. This is very likely the reason for the significant deviation between radiocarbon dates of the same layer and TL ages, because SAR and multiple-aliquot additive-dose (MAAD) ages of the same sample agree and other influencing variables such as the α-efficiency or the moisture content have too little impact on the calculated age as to explain the observed discrepancies. The SAR approach allowed dating the relatively small silex samples from the cave site Las Palomas (Spain). Here, successful dose recovery tests indicated the suitability of the measurement procedure, and in-situ measurements of γ-radiation provided more accurate dose rate information. As a result, TL ages between ~51 and ~84 ka allow a first chronometric assessment of the formerly undated archeological remains. Artefacts from the Aurignacian site Românești-Dumbrăvița I (Romania) proved to be more problematic, as part of them had to be discarded due to poor dose reproducibility. SAR measurements, dose recovery tests and their detailed analyses suggested internal non-uniformities of most samples, so that only rigorous data filtering allowed extraction of reliable age estimates. Due to the luminescence behavior of dated samples, the occupation of the site could, however, not be narrowed down to a range smaller than ~39-45 ka, giving a weighted average age of 40.6 ± 1.5 ka for the Aurignacian find layer. Furthermore, two TL emissions (blue and red) and two protocols (SAR and MAAD) were applied to heated silex from Sodmein Cave (Egypt). Dose recovery tests showed uncorrectable sensitivity changes of the TL signal, rendering the TL SAR sequence inaccurate for these samples. Consequently, age estimates are based on TL MAAD and OSL SAR data; for the smallest sample only a TL SAR maximum age can be given. Coming from different depths of a huge hearth, TL ages of dated samples indicate a large time span to be condensed in the archeological deposits, probably reaching from MIS 5e to MIS 5a.

A PDF of this thesis can be downloaded from http://kups.ub.uni-koeln.de/5109/

Bibliography
Compiled by Daniel Richter

_____

From 1ˢᵗ December 2012 to 31ˢᵗ May 2013

Alappat, L., Frechen, M., Tsukamoto, S., and Vink, A. (2012). Reply to 'Comment on: "Establishing the Late Pleistocene-Holocene sedimentation boundary in the southern North Sea using OSL dating of shallow continental shelf sediments" by L. Alappat, A. Vink, S. Tsukamoto, M. Frechen, Proceedings of the Geologists' Association 121 (2010), 43-54' by B. Mauz. *Proceedings of the Geologists Association* **123,** 666-668.

Amos, C. B., Lutz, A. T., Jayko, A. S., Mahan, S. A., Fisher, G. B., and Unruh, J. R. (2013). Refining the Southern Extent of the 1872 Owens Valley Earthquake Rupture through Paleoseismic Investigations in the Haiwee Area, Southeastern California. *Bulletin of the Seismological Society of America* **103,** 1022-1037.

Anthony, E. J., Mrani-Alaoui, M., and Héquette, A. (2012). Reply to the comment on "Shoreface sand supply and mid- to late Holocene aeolian dune formation on the storm dominated macrotidal coast of the southern North Sea" by E.J. Anthony, M. Mrani-Alaoui and A. Héquette [Marine Geology 276 (2010) 100–104]. *Marine Geology* **311–314,** 67-70.

Antoine, P., Rousseau, D.-D., Degeai, J.-P., Moine, O., Lagroix, F., kreutzer, S., Fuchs, M., Hatté, C., Gauthier, C., Svoboda, J., and Lisá, L. (2013). High-resolution record of the environmental response to climatic variations during the Last Interglacial–Glacial cycle in Central Europe: the loess-palaeosol sequence of Dolní Věstonice (Czech Republic). *Quaternary Science Reviews* **67,** 17-38.

Armitage, S. J., and King, G. E. (2013). Optically stimulated luminescence dating of hearths from the Fazzan Basin, Libya: A tool for determining the timing and pattern of Holocene occupation of the Sahara. *Quaternary Geochronology* **15,** 88-97.

Arnold, L. J., Demuro, M., Navazo, M., Benito-Calvo, A., and Pérez-González, A. (2013). OSL dating of the Middle Palaeolithic Hotel California site, Sierra de Atapuerca, north-central Spain. *Boreas* **42,** 285-305.

Avcioglu, M., Erginal, A. E., Kiyak, N. G., Kapan-Yesilyurt, S., and Yigitbas, E. (2013). A Preliminary Note on Depositional Characteristics and Optical Luminescence Age of a Marine Terrace, Strait of Canakkale, Turkey. *Journal of Coastal Research* **29,** 225-230.

Baeteman, C., and Mauz, B. (2012). Comments on "Shoreface sand supply and mid- to late Holocene aeolian dune formation on the storm-dominated macrotidal coast of the southern North Sea" by E.J. Anthony, M. Mrani-Alaoui and A. Héquette [Marine Geology 276 (2010) 100-104]. *Marine Geology* **311–314,** 63-66.

Bailiff, I. K., Lacey, H. R., Coningham, R. A. E., Gunawardhana, P., Adikari, G., Davis, C. E., Manuel, M. J., and Strickland, K. M. (2013). Luminescence dating of brick stupas: an application to the hinterland of Anuradhapura, Sri Lanka. *Antiquity* **87,** 189–201.

Bali, R., Nawaz Ali, S., Agarwal, K. K., Rastogi, S. K., Krishna, K., and Srivastava, P. (2013). Chronology of late Quaternary glaciation in the Pindar valley, Alaknanda basin, Central Himalaya (India). *Journal of Asian Earth Sciences* **66,** 224-233.

Baltrūnas, V., Šeirienė, V., Molodkov, A., Zinkutė, R., Katinas, V., Karmaza, B., Kisielienė, D., Petrošius, R., Taraškevičius, R., Piličiauskas, G., Schmölcke, U., and Heinrich, D. (2013). Depositional environment and climate changes during the late Pleistocene as recorded by the Netiesos section in southern Lithuania. *Quaternary International* **292,** 136-149.

Bhattacharya, F., Rastogi, B. K., Ngangom, M., Thakkar, M. G., and Patel, R. C. (2013). Late Quaternary climate and seismicity in the Katrol hill range, Kachchh, western India. *Journal of Asian Earth Sciences* **73,** 114-120.

Boroda, R., Matmon, A., Amit, R., Haviv, I., Porat, N., Aster, T., Rood, D., Eyal, Y., and Enzel, Y. (2013). Long-term talus flatirons formation in the hyperarid northeastern Negev, Israel. *Quaternary Research* **79,** 256-267.

Bridgland, D. R., Harding, P., Allen, P., Candy, I., Cherry, C., George, W., Horne, D. J., Keen, D. H., Penkman, K. E. H., Preece, R. C., Rhodes, E. J., Scaife, R., Schreve, D. C., Schwenninger, J.-L., Slipper, I., Ward, G. R., White, M. J., White, T. S., and Whittaker, J. E. (2013). An enhanced record of MIS 9 environments, geochronology and

geoarchaeology: data from construction of the High Speed 1 (London-Channel Tunnel) rail-link and other recent investigations at Purfleet, Essex, UK. *Proceedings of the Geologists Association* **124,** 417-476.

Cano, N. F., Machado, N. T. G., Gennari, R. F., Rocca, R. R., Munita, C. S., and Watanabe, S. (2012). TL dating of pottery fragments from four archaeological sites in Taquari Valley, Brazil. *Radiation Effects and Defects in Solids* **167,** 947-953.

Chen, G.-Q., Yi, L., Xu, X.-Y., Yu, H.-J., Cao, J.-R., Su, Q., Yang, L.-H., Xu, Y.-H., Ge, J.-Y., and Lai, Z.-P. (2013). Testing the standardized growth curve (SGC) to OSL dating coastal sediments from the south Bohai Sea, China. *Geochronometria* **40,** 101-112.

Chen, Y., Li, S.-H., Sun, J., and Fu, B. (2013). OSL dating of offset streams across the Altyn Tagh Fault: Channel deflection, loess deposition and implication for the slip rate. *Tectonophysics* **594,** 182-194.

Corcea, C. A., Constantin, D., Anechitei, V., Timar-Gabor, A., and Filipescu, S. (2013). SAR OSL dating of 63-90 μm quartz extracted from an Eemian (presumably lacustrine) sedimentary section at Floresti on the Somesul Mic Valley. *Carpathian Journal of Earth and Environmental Sciences* **8,** 139-145.

Czopek, S., Kusiak, J., and Trybała-Zawiślak, K. (2013). Thermoluminescent dating of the Late Bronze and Early Iron Age pottery on sites in Kłyżów and Jarosław (SE Poland). *Geochronometria* **40,** 113-125.

Demuro, M., Arnold, L. J., Froese, D. G., and Roberts, R. G. (2013). OSL dating of loess deposits bracketing Sheep Creek tephra beds, northwest Canada: Dim and problematic single-grain OSL characteristics and their effect on multi-grain age estimates. *Quaternary Geochronology* **15,** 67-87.

Dibble, H. L., Aldeias, V., Alvarez-Fernández, E., Blackwell, B., Hallett-Desguez, E., Jacobs, Z., Goldberg, P., Lin, S. C., Morala, A., Meyer, M. C., Olzsewski, D. I., Reed, K., Reed, D., Rezek, Z., Richter, D., Roberts, R. G., Sandgathe, D., Schurmans, U., Skinner, A., Steele, T., and El-Hajraoui, M. (2012). New Excavations at the Site of Contrebandiers Cave, Morocco. *PaleoAnthropology* **2012,** 145-201.

Erginal, A. E., Kiyak, N. G., Ekinci, Y. L., Demirci, A., Ertek, A., and Canel, T. (2013). Age, composition and paleoenvironmental significance of a Late Pleistocene eolianite from the western Black Sea coast of Turkey. *Quaternary International* **296,** 168-175.

Erginal, A. E., Kiyak, N. G., Ozturk, M. Z., Avcioglu, M., Bozcu, M., and Yigitbas, E. (2012). Cementation characteristics and age of beachrocks in a fresh-water environment, Lake Iznik, NW Turkey. *Sedimentary Geology* **243,** 148-154.

Fedorowicz, S., Łanczont, M., Bogucki, A., Kusiak, J., Mroczek, P., Adamiec, G., Bluszcz, A., Moska, P., and Tracz, M. (2013). Loess-paleosol sequence at Korshiv (Ukraine): Chronology based on complementary and parallel dating (TL, OSL), and litho-pedosedimentary analyses. *Quaternary International* **296,** 117-130.

Forsyth, A. J., Nott, J., Bateman, M. D., and Beaman, R. J. (2012). Juxtaposed beach ridges and foredunes within a ridge plain — Wonga Beach, northeast Australia. *Marine Geology* **307–310,** 111-116.

Frochoso, M., Gonzalez-Pellejero, R., and Allende, F. (2013). Pleistocene glacial morphology and timing of last glacial cycle in cantabrian mountains (Northern Spain): new chronological data from the Asn area. *Central European Journal of Geosciences* **5,** 12-27.

Gattuso, C., Renzelli, D., Barone, P., Pingitore, V., and Oliva, A. (2012). SAR and MAAD TL dating of "Caroselu" from three sites in Calabria, South Italy. *Mediterranean Archaeology and Archaeometry* **12,** 43-54.

Gerardi, F., Smedile, A., Pirrotta, C., Barbano, M. S., De Martini, P. M., Pinzi, S., Gueli, A. M., Ristuccia, G. M., Stella, G., and Troja, S. O. (2012). Geological record of tsunami inundations in Pantano Morghella (south-eastern Sicily) both from near and far-field sources. *Natural Hazards and Earth System Sciences* **12,** 1185-1200.

Guérin, G., Murray, A. S., Jain, M., Thomsen, K. J., and Mercier, N. (2013). How confident are we in the chronology of the transition between Howieson's Poort and Still Bay? *Journal of Human Evolution* **64,** 314-317.

Guhl, A., Bertran, P., Zielhofer, C., and Fitzsimmons, K. E. (2013). Optically Stimulated Luminescence (OSL) dating of sand-filled wedge structures and their fine-grained host sediment from Jonzac, SW France. *Boreas* **42,** 317-332.

Gurgel, S. P. P., Bezerra, F. H. R., Corrêa, A. C. B., Marques, F. O., and Maia, R. P. (2013). Cenozoic uplift and erosion of structural landforms in NE Brazil. *Geomorphology* **186,** 68-84.

Hall, S. A., and Goble, R. J. (2012). Berino Paleosol, Late Pleistocene Argillic Soil Development on the Mescalero Sand Sheet in New Mexico. *Journal of Geology* **120,** 333-345.

Hérisson, D., Airvaux, J., Lenoble, A., Richter, D., Claud, E., and Primault, J. (2012). Le gisement acheuléen de la Grande Vallée à Colombiers (Vienne, France): stratigraphie, processus de formation, datations préliminaires et industries lithiques. *Paléo* **23,** 137-154.

Holmes, P. J., Thomas, D. S. G., Bateman, M. D., Wiggs, G. F. S., and Rabumbulu, M. (2012). Evidence for land degradation from aeolian sediment in the West-Central Free State Province, Ssouth Aafrica. *Land Degradation & Development* **23,** 601-610.

Hong, H., Gu, Y., Yin, K., Wang, C., and Li, Z. (2013). Clay record of climate change since the mid-Pleistocene in Jiujiang, south China. *Boreas* **42,** 173-183.

Houben, P., Schmidt, M., Mauz, B., Stobbe, A., and Lang, A. (2013). Asynchronous Holocene colluvial and alluvial aggradation: A matter of hydrosedimentary connectivity. *The Holocene* **23,** 544-555.

Hu, Z., Pan, B., Wang, J., Cao, B., and Gao, H. (2012). Fluvial terrace formation in the eastern Fenwei Basin, China, during the past 1.2 Ma as a combined archive of tectonics and climate change. *Journal of Asian Earth Sciences* **60,** 235-245.

Huang, C. C., Pang, J., Zha, X., Zhou, Y., Yin, S., Su, H., Zhou, L., and Yang, J. (2013). Extraordinary hydro-climatic events during the period AD 200−300 recorded by slackwater deposits in the upper Hanjiang River valley, China. *Palaeogeography, Palaeoclimatology, Palaeoecology* **374,** 274-283.

Huckleberry, G., Onken, J., Graves, W. M., and Wegener, R. (2013). Climatic, geomorphic, and archaeological implications of a late Quaternary alluvial chronology for the lower Salt River, Arizona, USA. *Geomorphology* **185,** 39-53.

Kadereit, A., and Kreutzer, S. (2013). Risø calibration quartz − A challenge for β-source calibration. An applied study with relevance for luminescence dating. *Measurement* **46,** 2238-2250.

Keen-Zebert, A., Tooth, S., Rodnight, H., Duller, G. A. T., Roberts, H. M., and Grenfell, M. (2013). Late Quaternary floodplain reworking and the preservation of alluvial sedimentary archives in unconfined and confined river valleys in the eastern interior of South Africa. *Geomorphology* **185,** 54-66.

Kusiak, J., Łanczont, M., Madeyska, T., and Bogucki, A. (2013). Problems of TL dating of the Mesopleistocene loess deposits in the Podillya and Pokuttya regions (Ukraine). *Geochronometria* **40,** 51-58.

Lahaye, C., Hernandez, M., Boëda, E., Felice, G. D., Guidon, N., Hoeltz, S., Lourdeau, A., Pagli, M., Pessis, A.-M., Rasse, M., and Viana, S. (2013). Human occupation in South America by 20,000 BC: the Toca da Tira Peia site, Piauí, Brazil. *Journal of Archaeological Science* **40,** 2840-2847.

Lamotte, A., Aubry, D., Debenham, N., Magniez, P., Le Mené, F., and Galtier, F. (2012). Le gisement paléolithique de Pont-de-Planches (Haute-Saône, France) : cadre paléoenvironnemental et datations des occupations du Paléolithique moyen et Paléolithique supérieur. *Quaternaire* **23,** 291-308.

Łanczont, M., Bogucki, A., Kusiak, J., and Sytnyk, O. (2013). The results of thermoluminescence dating in the Halych IIC (Ukraine) profile as the expression of the conditions of mineral material deposition. *Geochronometria* **40,** 42-50.

Lim, J., Kim, J.-Y., Kim, S.-J., Lee, J.-Y., and Hong, S.-S. (2013). Late Pleistocene vegetation change in Korea and its possible link to East Asian monsoon and Dansgaard–Oeschger (D–O) cycles. *Quaternary Research* **79,** 55-60.

Liu, X.-J., and Lai, Z.-P. (2013). Optical dating of sand wedges and ice-wedge casts from Qinghai Lake area on the northeastern Qinghai-Tibetan Plateau and its palaeoenvironmental implications. *Boreas* **42,** 333-341.

Lovis, W. A., Monaghan, G. W., Arbogast, A. F., and Forman, S. L. (2012). Differential Temporal and Spatial Preservation of Archaeological Sites in a Great Lakes Coastal Zone. *American Antiquity* **77,** 591-608.

Luirei, K., Bhakuni, S. S., Srivastava, P., and Suresh, N. (2012). Late Pleistocene - Holocene tectonic activities in the frontal part of NE Himalaya between Siang and Dibang river valleys, Arunachal Pradesh, India. *Zeitschrift für Geomorphologie* **56,** 477-493.

Macklin, M. G., Woodward, J. C., Welsby, D. A., Duller, G. A. T., Williams, F. M., and Williams, M. A. J. (2013). Reach-scale river dynamics moderate the impact of rapid Holocene climate change on floodwater farming in the desert Nile. *Geology* **41,** 695-698.

Markewich, H. W., Pavich, M. J., Schultz, A. P., Mahan, S. A., Aleman-Gonzalez, W. B., and Bierman, P. R. (2013). Geochronologic evidence for a possible MIS-11 emergent barrier/beach-ridge in southeastern Georgia, USA. *Quaternary Science Reviews* **60,** 49-75.

Mauz, B. (2012). Comment on: "Establishing the Late Pleistocene-Holocene sedimentation boundary in the southern North Sea using OSL dating of shallow continental shelf sediments" by L. Alappat, A. Vink, S. Tsukamoto, M. Frechen, Proceedings of the Geologists' Association 121 (2010) 43-54. *Proceedings of the Geologists Association* **123,** 663-665.

McIlvenny, J. D., Muller, F. L. L., and Dawson, A. (2013). A 7600-year sedimentary record of climatic instability in Dunnet Bay, North Scotland. *Marine Geology* **335,** 100-113.

Meszner, S., Kreutzer, S., Fuchs, M., and Faust, D. (2013). Late Pleistocene landscape dynamics in Saxony, Germany: Paleoenvironmental reconstruction using loess-paleosol sequences. *Quaternary International* **296,** 94-107.

Miallier, D., Pilleyre, T., Sanzelle, S., Boivin, P., and Lanos, P. (2012). Revised chronology of the youngest volcanoes of the chaîne des puys (french Massif central). *Quaternaire* **23,** 283-290.

Möller, P., Anjar, J., and Murray, A. S. (2013). An OSL-dated sediment sequence at Idre, west-central Sweden, indicates ice-free conditions in MIS 3. *Boreas* **42,** 25-42.

Moska, P., and Bluszcz, A. (2013). Luminescence dating of loess profiles in Poland. *Quaternary International* **296,** 51-60.

Munyikwa, K., Brown, S., and Kitabwalla, Z. (2012). Delineating stratigraphic breaks at the bases of postglacial eolian dunes in central Alberta, Canada using a portable OSL reader. *Earth Surface Processes and Landforms* **37,** 1603-1614.

Pan, B., Hu, X., Gao, H., Hu, Z., Cao, B., Geng, H., and Li, Q. (2013). Late Quaternary river incision rates and rock uplift pattern of the eastern Qilian Shan Mountain, China. *Geomorphology* **184,** 84-97.

Pascucci, V., Panzeri, L., Martini, M., Maspero, F., Sechi, D., and Andreucci, S. (2012). Is Optically Stimulated Luminescence a reliable tool for dating the Quaternary paleoenvironmental evolution? the case of Argentiera (NW-Sardinia, Italy). *Rendiconti Online Societa Geologica Italiana* **21,** 911-912.

Pederson, J. L., Cragun, W. S., Hidy, A. J., Rittenour, T. M., and Gosse, J. C. (2013). Colorado River chronostratigraphy at Lee's Ferry, Arizona, and the Colorado Plateau bull's-eye of incision. *Geology* **41,** 427-430.

Pflanz, D., Gaedicke, C., Freitag, R., Krbetschek, M., Tsukanov, N., and Baranov, B. (2013). Neotectonics and recent uplift at Kamchatka and Aleutian arc junction, Kamchatka Cape area, NE Russia. *International Journal of Earth Sciences* **102,** 903-916.

Phartiyal, B., and Kothyari, G. C. (2012). Impact of neotectonics on drainage network evolution reconstructed from morphometric indices: case study from NW Indian Himalaya. *Zeitschrift für Geomorphologie* **56,** 121-140.

Pickering, R., Jacobs, Z., Herries, A. I. R., Karkanas, P., Bar-Matthews, M., Woodhead, J. D., Kappen, P., Fisher, E., and Marean, C. W. (2013). Paleoanthropologically significant South African sea caves dated to 1.1–1.0 million years using a combination of U–Pb, TT-OSL and palaeomagnetism. *Quaternary Science Reviews* **65,** 39-52.

Poręba, G. J., Śnieszko, Z., and Moska, P. (2013). Influence of pedon history and washing nature on luminescence dating of Holocene colluvium on the example of research on the Polish loess areas. *Quaternary International* **296,** 61-67.

Preusser, F., Kock, S., and Rodnight, H. (2012). Comment on Frechen et al. "Late Pleistocene fluvial dynamics in the Hochrhein Valle and in the Upper Rhine Graben: chronological frame". *International Journal of Earth Sciences* **101,** 385-387.

Puta, R. A., Hanson, P. R., and Young, A. R. (2013). Late Holocene Activation History of the Stanton Dunes, Northeastern Nebraska. *Great Plains Research* **23,** 11-23.

Qiang, M., Chen, F., Song, L., Liu, X., Li, M., and Wang, Q. (2013). Late Quaternary aeolian activity in Gonghe Basin, northeastern Qinghai-Tibetan Plateau, China. *Quaternary Research* **79,** 403-412.

Rich, J. (2013). A 250,000-year record of lunette dune accumulation on the Southern High Plains, USA and implications for past climates. *Quaternary Science Reviews* **62,** 1-20.

Richter, D., Dibble, H., Goldberg, P., McPherron, S., Niven, L., Sandgathe, D., Talamo, S., and Turq, A. (2013). The Late Middle Palaeolithic in Southwest France: New TL dates for the sequence of Pech de l'Azé IV. *Quaternary International* **294,** 160–167.

Rink, W. J., Dunbar, J. S., Tschinkel, W. R., Kwapich, C., Repp, A., Stanton, W., and Thulman, D. K. (2013). Subterranean transport and deposition of quartz by ants in sandy sites relevant to age overestimation in optical luminescence dating. *Journal of Archaeological Science* **40,** 2217-2226.

Rizza, M., Vernant, P., Ritz, J. F., Peyret, M., Nankali, H., Nazari, H., Djamour, Y., Salamati, R., Tavakoli, F., Chéry, J., Mahan, S. A., and Masson, F. (2013). Morphotectonic and geodetic evidence for a constant slip-rate over the last 45 kyr along the Tabriz fault (Iran). *Geophysical Journal International* **193,** 1083-1094.

Rosentau, A., Joeleht, A., Plado, J., Aunap, R., Muru, M., and Eskola, K. O. (2013). Development of the holocene foredune plain in the Narva-Joesuu area, eastern Gulf of Finland. *Geological Quarterly* **57,** 89-100.

Roy, M., Allard, G., Lamothe, M., and Veillette, J. J. (2013). Glacial and nonglacial events in the eastern James Bay lowlands, Canada. *Canadian Journal of Earth Sciences* **50,** 379-396.

Ryb, U., Matmon, A., Porat, N., and Katz, O. (2013). From mass-wasting to slope stabilization – putting constrains on a tectonically induced transition in slope erosion mode: a case study in the Judea Hills, Israel. *Earth Surface Processes and Landforms* **38,** 551-560.

Şahiner, E., Meriç, N., and Uygun, S. (2013). Luminescence (IRSL) dating of Yeni Rabat church in Artvin, Turkey. *Radiation Physics and Chemistry* **86,** 68-73.

Sanjurjo-Sánchez, J., Alves, C., and Lobarinhas, D. (2012). Estimating the age of lime mortars by luminescence to measure pollution rates. *Materials Science Forum* **730-732,** 598-603.

Satkunas, J., Grigiene, A., Buynevich, I. V., and Taminskas, J. (2013). A new Early–Middle Weichselian palaeoenvironmental record from a lacustrine sequence at Svirkanciai, Lithuania. *Boreas* **42,** 184-193.

Schmidt, C., and Kreutzer, S. (2013). Optically stimulated luminescence of amorphous/microcrystalline SiO_2 (silex): Basic investigations and potential in archeological dosimetry. *Quaternary Geochronology* **15,** 1-10.

Schmidt, C., Rufer, D., Preusser, F., Krbetschek, M., and Hilgers, A. (2013). The assessment of radionuclide distribution in silex by autoradiography in the context of dose rate determination for thermoluminescence dating *Archaeometry* **55,** 407-422.

Schreve, D., Howard, A., Currant, A., Brooks, S., Buteux, S., Coope, R., Crocker, B., Field, M., Greenwood, M., Greig, J., and Toms, P. (2013). A Middle Devensian woolly rhinoceros (Coelodonta antiquitatis) from Whitemoor Haye Quarry, Staffordshire (UK): palaeoenvironmental context and significance. *Journal of Quaternary Science* **28,** 118-130.

Sears, D. W. G., Ninagawa, K., and Singhvi, A. K. (2013). Luminescence studies of extraterrestrial materials: Insights into their recent radiation and thermal histories and into their metamorphic history. *Chemie der Erde - Geochemistry* **73,** 1-37.

Seminack, C. T., and Buynevich, I. V. (2013). Sedimentological and Geophysical Signatures of A Relict Tidal Inlet Complex Along A Wave-Dominated Barrier: Assateague Island, Maryland, U.S.A. *Journal of Sedimentary Research* **83,** 104-116.

Shanahan, T. M., Peck, J. A., McKay, N., Heil Jr, C. W., King, J., Forman, S. L., Hoffmann, D. L., Richards, D. A., Overpeck, J. T., and Scholz, C. (2013). Age models for long lacustrine sediment records using multiple dating approaches – An example from Lake Bosumtwi, Ghana. *Quaternary Geochronology* **15,** 47-60.

Shirai, M., and Hayashizaki, R. (2013). Transport process of sand grains from fluvial to deep marine regions estimated by luminescence of feldspar: example from the Kumano area, central Japan. *Island Arc* **22,** 242-257.

Sirocko, F., Dietrich, S., Veres, D., Grootes, P. M., Schaber-Mohr, K., Seelos, K., Nadeau, M.-J., Kromer, B., Rothacker, L., Röhner, M., Krbetschek, M., Appleby, P., Hambach, U., Rolf, C., Sudo, M., and Grim, S. (2013). Multi-proxy dating of Holocene maar lakes and Pleistocene dry maar sediments in the Eifel, Germany. *Quaternary Science Reviews* **62,** 56-76.

Sitlivy, V., Chabai, V., Anghelinu, M., Uthmeier, T., Kels, H., Hilgers, A., Schmidt, C., Niţă, L., Băltean, I., Veselsky, A., and Hauck, T. (2012). The earliest Aurignacian in Romania: New investigations at the open air site of Românești-Dumbrăviţa I (Banat). *Quartär* **59**. 85-130.

Sohbati, R., Murray, A., Jain, M., Thomsen, K., Hong, S.-C., Yi, K., and Choi, J.-H. (2013). Na-rich feldspar as a luminescence dosimeter in infrared stimulated luminescence (IRSL) dating. *Radiation Measurements* **51–52,** 67-82.

Sridhar, A., Chamyal, L. S., Bhattacharjee, F., and Singhvi, A. K. (2013). Early Holocene fluvial activity from the sedimentology and palaeohydrology of gravel terrace in the semi arid Mahi River Basin, India. *Journal of Asian Earth Sciences* **66,** 240-248.

Starnberger, R., Drescher-Schneider, R., Reitner, J. M., Rodnight, H., Reimer, P. J., and Spötl, C. (2013). Late Pleistocene climate change and landscape dynamics in the Eastern Alps: the inner-alpine Unterangerberg record (Austria). *Quaternary Science Reviews* **68,** 17-42.

Stockmann, U., Minasny, B., Pietsch, T. J., and McBratney, A. B. (2013). Quantifying processes of pedogenesis using optically stimulated luminescence. *European Journal of Soil Science* **64,** 145-160.

Stone, A. E. C., and Thomas, D. S. G. (2013). Casting new light on late Quaternary environmental and palaeohydrological change in the Namib Desert: A review of the application of optically stimulated luminescence in the region. *Journal of Arid Environments* **93,** 40-58.

Sun, X., Lu, H., Wang, S., Yi, S., Shen, C., and Zhang, W. (2013). TT-OSL dating of Longyadong Middle Paleolithic site and paleoenvironmental implications for hominin occupation in Luonan Basin (central China). *Quaternary Research* **79,** 168-174.

Sun, X., Lu, H., Yi, S., and Bahain, J. J. (2013). Age and paleoenvironment of Paleolithic stone artifact remains discovered in the Tengger Desert, northern China. *Journal of Arid Environments* **91,** 129-137.

Tema, E., Fantino, F., Ferrara, E., Lo Giudice, A., Morales, J., Goguitchaichvili, A., Camps, P., Barello, F., and Gulmini, M. (2013). Combined archaeomagnetic and thermoluminescence study of a brick kiln excavated at Fontanetto Po (Vercelli, Northern Italy). *Journal of Archaeological Science* **40,** 2025-2035.

Thalbitzer Andersen, M., Jain, M., and Tidemand-Lichtenberg, P. (2012). Red-IR stimulated luminescence in K-feldspar: Single or multiple trap origin? *Journal of Applied Physics* **112**, 043507.

Tolksdorf, J. F., Klasen, N., and Hilgers, A. (2013). The existence of open areas during the Mesolithic: evidence from aeolian sediments in the Elbe–Jeetzel area, northern Germany. *Journal of Archaeological Science* **40,** 2813-2823.

Topaksu, M., Yüksel, M., Dogan, T., Nur, N., Akkaya, R., Yegingil, Z., and Topak, Y. (2013). Investigation of the characteristics of thermoluminescence glow curves of natural hydrothermal quartz from Hakkari area in Turkey. *Physica B: Condensed Matter* **424,** 27-31.

Tronchere, H., Goiran, J.-P., Schmitt, L., Preusser, F., Bietak, M., Forstner-Mueller, I., and Callot, Y. (2012). Geoarchaeology of an ancient fluvial harbour: Avaris and the Pelusiac branch (Nile River, Egypt). *Géomorphologie - Relief Processus Environnement* **2012/1**, 23-36.

Tsatskin, A., Sandler, A., and Porat, N. (2013). Toposequence of sandy soils in the northern coastal plain of Israel: Polygenesis and complexity of pedogeomorphic development. *Geoderma* **197–198,** 87-97.

Tseng, C.-H., Wenske, D., Böse, M., Reimann, T., Lüthgens, C., and Frechen, M. (2013). Sedimentary features and ages of fluvial terraces and their implications for geomorphic evolution of the Taomi River catchment: A case study in the Puli Basin, central Taiwan. *Journal of Asian Earth Sciences* **62,** 759-768.

Turner, F., Tolksdorf, J. F., Viehberg, F., Schwalb, A., Kaiser, K., Bittmann, F., von Bramann, U., Pott, R., Staesche, U., Breest, K., and Veil, S. (2013). Lateglacial/early Holocene fluvial reactions of the Jeetzel river (Elbe valley, northern Germany) to abrupt climatic and environmental changes. *Quaternary Science Reviews* **60,** 91-109.

Tylmann, W., Enters, D., Kinder, M., Moska, P., Ohlendorf, C., Poręba, G., and Zolitschka, B. (2013). Multiple dating of varved sediments from Lake Łazduny, northern Poland: Toward an improved chronology for the last 150 years. *Quaternary Geochronology* **15,** 98-107.

Vandenberghe, D. A. G., Derese, C., Kasse, C., and Van den haute, P. (2013). Late Weichselian (fluvio-)aeolian sediments and Holocene drift-sands of the classic type locality in Twente (E Netherlands): a high-resolution dating study using optically stimulated luminescence. *Quaternary Science Reviews* **68,** 96-113.

Vasiliniuc, Ş., Vandenberghe, D. A. G., Timar-Gabor, A., Cosma, C., and van den Haute, P. (2013). Combined IRSL and post-IR OSL dating of Romanian loess using single aliquots of polymineral fine grains. *Quaternary International* **293,** 15-21.

Veres, D., Lane, C. S., Timar-Gabor, A., Hambach, U., Constantin, D., Szakács, A., Fülling, A., and Onac, B. P. (2013). The Campanian Ignimbrite/Y5 tephra layer – A regional stratigraphic marker for Isotope Stage 3 deposits in the Lower Danube region, Romania. *Quaternary International* **293,** 22-33.

Viveen, W., Braucher, R., Bourles, D., Schoorl, J. M., Veldkamp, A., van Balen, R. T., Wallinga, J., Fernandez-Mosquera, D., Vidal-Romani, J. R., and Sanjurjo-Sanchez, J. (2012). A 0.65 Ma chronology and incision rate assessment of the NW Iberian Mino River terraces based on Be-10 and luminescence dating. *Global and Planetary Change* **94-95,** 82-100.

Voelkel, J., Grunert, J., Leopold, M., Huerkamp, K., Huber, J., and Murray, A. (2013). Eolian and fluvial sedimentation in the southwestern Sinai Mountains, Egypt: a record of flash floods during the late Pleistocene. *Hydrology Research* **44,** 281-299.

Wang, J., Pan, B., Zhang, G., Cui, H., Cao, B., and Geng, H. (2013). Late Quaternary glacial chronology on the eastern slope of Gongga Mountain, eastern Tibetan Plateau, China. *Science China Earth Sciences* **56,** 354-365.

Wang, X. L., and Wintle, A. G. (2013). Investigating the contribution of recuperated TL to post-IR IRSL signals in a perthitic feldspar. *Radiation Measurements* **49,** 82-87.

Wasson, R. J., Chauhan, M. S., Sharma, C., Jaiswal, M., Singhvi, A. K., and Srivastava, P. (2013). Erosion of river terraces as a component of large catchment sediment budgets: A pilot study from the Gangetic Plain. *Journal of Asian Earth Sciences* **67–68,** 18-25.

Weckwerth, P., Przegietka, K. R., Chruścińska, A., and Pisarska-Jamrozy, M. (2013). The relation between optical bleaching and sedimentological features of fluvial deposits in the Toruń basin (Poland). *Geological Quarterly* **57,** 31-44.

Wen-Jun, Z., Hui-Ping, Z., Pei-Zhen, Z., Molnar, P., Xing-Wang, L., and Dao-Yang, Y. (2013). Late Quaternary slip rates of the thrust faults in western Hexi Corridor (Northern Qilian Shan, China) and their implications for northeastward growth of the Tibetan Plateau. *Geosphere* **9,** 342-354.

Yang, L.-R., and Ding, Z.-L. (2013). Expansion and contraction of Hulun Buir Dunefield in north-eastern China in the last late glacial and Holocene as revealed by OSL dating. *Environmental Earth Sciences* **68,** 1305-1312.

Yang, X., Li, A., and Hunag, W. (2013). Uplift differential of active fold zones during the late Quaternary, northern piedmonts of the Tianshan Mountains, China. *Science China Earth Sciences* **56,** 794-805.

Yi, L., Lai, Z., Yu, H., Xu, X., Su, Q., Yao, J., Wang, X., and Shi, X. (2013). Chronologies of sedimentary changes in the south Bohai Sea, China: constraints from luminescence and radiocarbon dating. *Boreas* **42,** 267-284.

Zander, A., and Hilgers, A. (2013). Potential and limits of OSL, TT-OSL, IRSL and pIRIR(290) dating methods applied on a Middle Pleistocene sediment record of Lake El'gygytgyn, Russia. *Climate of the Past* **9,** 719-733.

Zha, X., Huang, C., Pang, J., and Li, Y. (2012). Sedimentary and hydrological studies of the Holocene palaeofloods in the middle reaches of the Jinghe River. *Journal of Geographical Sciences* **22,** 470-478.

Zhang, W., He, M., Li, Y., Cui, Z., Wang, Z., and Yu, Y. (2012). Quaternary glacier development and the relationship between the climate change and tectonic uplift in the Helan Mountain. *Chinese Science Bulletin* **57,** 4491-4504.

Zink, A. (2013). A coarse Bayesian approach to evaluate luminescence ages. *Geochronometria* **40,** 90-100.

Zular, A., Sawakuchi, A. O., Guedes, C. C. F., Mendes, V. R., Nascimento Jr, D. R., Giannini, P. C. F., Aguiar, V. A. P., and DeWitt, R. (2013). Late Holocene intensification of colds fronts in southern Brazil as indicated by dune development and provenance changes in the São Francisco do Sul coastal barrier. *Marine Geology* **335,** 64-77.

Conference Announcements

14th International Conference on Luminescence and Electron Spin Resonance Dating (LED 2014)

7th-11th July 2014

The Lux laboratory team, at the Université du Québec à Montréal, is inviting you to participate in the 14th International Conference on Luminescence and Electron Spin Resonance Dating (LED 2014).

The conference will take place at the New Residence Hall (**http://www.mcgill.ca/nrh**) in Montreal, Canada, between July 7th and 11th 2014. An icebreaker reception will be held in the lounge of the NRH, on July 6th.

The conference will be followed by an optional 2-day (12th to 13th July 2014) geological and archaeological field trip that will bring the participants along the St. Lawrence River Valley, looping through Québec City and the agricultural countryside of Southern Québec.

The conference hopes to attract a large array of fundamental as well as applied research presentations. The technical sessions should be of interest to researchers improving dating methodologies as well as to those using trapped charge dating techniques to solve geochronological problems. The topics include heated and unheated Quaternary geological, geomorphological and archaeological materials, luminescence basic physical phenomena dosimetry and advances in instrumentation.

Workshop

The meeting being held in Montréal, a special feldspar workshop might be organized, covering the mineralogy, crystallography, geological contexts and what we know of their solid state physics.

We would like to know if you would be interested in attending a workshop. If so, please let us know:
a) which themes would appeal to you
b) if you would prefer to have it on Sunday the 6th, before the icebreaker or early in the mornings during the conference.

Other suggestions are welcome.

General information

The web page of the conference will be online soon, and you can reach us by email at **LED2014@uqam.ca**. The online registration opens in late autumn 2013. The second circular will be sent in September 2013 *only to those who will express their desire to receive it*.

The organisers have guaranteed a large number of places for LED participant at the New Residence Hall hotel, at a cost of **114 $CAD/night** ATI.

The location

Montréal is internationally renowned for its cosmopolitan urban adventure, its world cuisine, its artistic and fun night life. Montréal is the host to many events and festivals, held throughout the year. In particular, we synchronized the start of LED 2014 with the end of the 35th edition of the International Jazz Festival (**http://www.montrealjazzfest.com/default-en.aspx**), which will be held between June 27th and July 6th.

Montréal will surely meet every expectation with its numerous museums, churches, historic sites, science centers, urban parks, and multicultural quarters.

On behalf of the organising Committee of LED 2014

Conference Announcements

German Luminescence and ESR meeting

Technical University of Freiberg & Freiberg Instruments

25-27th October 2013

The annual German Luminescence and ESR meeting will be held in Freiberg 25-27th October 2013 and is jointly organized by the Technical University of Freiberg and Freiberg Instruments. Although aimed primarily at the German speaking luminescence community many presentations are given in English and it is open to participants from all over the world.

The meeting is intended to provide a forum for research in trapped charge dating and related topics, with presentations covering basic physics, methodological issues and the application of relevant techniques. Especially students are encouraged to present their (preliminary) work as oral or poster presentations.

Following the long standing tradition of the German meeting, we will have three half days for presentations, suspended for an afternoon of hiking. One session of this meeting will be held in memory of Matthias Krbetschek, and we would especially welcome contributions focusing on his research topics.

Details can be found in the 2nd circular under NEWS at **http://www.lexsyg.com/**

Registration for participation and scientific contributions (oral or poster) as well as queries are welcome to **gLED@freiberginstruments.com** until September 15th.

Submission of articles to Ancient TL

Reviewing System

In order to ensure acceptable standards and minimize delay in publication, a modification of the conventional refereeing system has been devised for Ancient TL:

Articles can be sent directly by authors to a member of the Reviewers Panel chosen on the basis of the subject matter, but who is not in any of the authors' laboratories. **At the discretion of the Editor**, reviewers who are not listed in the Panel may be used.

The reviewing system aims to encourage direct dialogue between author and reviewer. The Editor should be kept advised of the progress of articles under review by sending him copies of all correspondence. He is available for advice where reviewing difficulties have arisen. Authors whose mother tongue is not English are required to have their manuscript revised for English *before* submitting it.

We ask reviewers to specify (where required) the minimum of revision that is consistent with achieving a clear explanation of the subject of the paper, the emphasis being on *rapid* publication; reviewers are encouraged to make a brief written comment for publication at the end of the paper. Where a contribution is judged not to meet an adequate standard without substantial modification, the author will be advised that the contribution is not suitable for publication. Articles that are not considered to be of sufficient interest may also be rejected.

Procedures

1. Articles should be submitted to an appropriate member of the Reviewing Panel or Editorial Board, chosen on the basis of the subject matter, but who is not in any of the authors' laboratories.
2. Articles should not normally exceed the equivalent of 5000 words inclusive of diagrams, tables and references. Greater space will be appropriate for certain topics; for these the Editor should first be consulted.
   Short notes and letters are also invited. These should not exceed two printed pages in Ancient TL, including diagrams, tables and references (equivalent to ~1400 words of text).
3. Diagrams and labels should be ready for direct reproduction and not normally exceed 12 cm wide by 10 cm high. Where possible, high quality electronic versions of figures should be submitted. Separate figure captions should be supplied. Inappropriately scaled drawings and labels will be returned for alteration.
4. Authors are asked to submit the paper, including diagrams, to the Reviewer and a duplicate copy to the Editor.
   The final version of the text must be submitted to the Editor electronically using a standard format (Microsoft Word for PC is currently used for producing Ancient TL). Electronic copies of Diagrams and Tables should also be submitted.
5. Upon receipt of an article, the Editor will send an acknowledgement to the author. If the Reviewer is unable to deal with the contribution within **4 weeks** he/she will inform the author and advise the Editor.

Requirements under various situations

When agreement concerning an article has been reached:
The Editor should receive a copy of the final version of the paper, both as hard copy and electronically. The Reviewer should send their final decision, including comments for publication if any, to the Editor.

If the article has not been rejected, but agreement on its final form cannot be reached or where there are protracted delays in the reviewing process:
The Editor may request an assessment from the Reviewer and responsibility passes to the Editor.

If the article is rejected:
The Editor and author receive notification from the Reviewer, with an indication of the reason for rejection.

Thesis abstracts are to be sent to the Editor and in principle do not need reviewing. However, authors are requested to make sure that the English is correct before submission. Thesis abstracts should not exceed 750 words, and figures and tables are not accepted.

Advertising. Formal information on equipment can be published in Ancient TL. It should not exceed one printed page. Current charges are displayed on the website (http://www.aber.ac.uk/ancient-tl)

Subscriptions to Ancient TL

Ancient TL is published 2 times a year and is sent Airmail to subscribers outside the United Kingdom. While every attempt will be made to keep to publication schedule, the Editorial Board may need to alter the number and frequency of issues, depending on the number of available articles which have been accepted by reviewers.

The subscription rate for 2013 is £15 for individual subscribers and £25 for Institutional subscription, plus any taxes where required. Payment must be in pounds sterling. Enquiries and orders must be sent to the Editor. Payment may be by cheques, made payable to 'Aberystwyth University', by credit/debit cards or by bank transfers. Further information on subscriptions is available on the Ancient TL web site (http://www.aber.ac.uk/ancient-tl)